Universiteit Utrecht

February 20, 2023

Synthesis of oseltamivir derivatives designed for multivalent influenza A inhibition

S. Molenberg[1] and Prof. Dr. R.J. Pieters[1]

[1]Chemical Biology and Drug Discovery, Utrecht University, Utrecht, The Netherlands

Abstract

As mutations within the influenza A virus have been leading to increased resistance against current monovalent neuraminidase inhibitors (NAIs) such as oseltamivir, research into the potential of multivalent NAIs has been gaining attention. The concept of multivalency has been proposed as an answer to the increased resistance since it could improve the efficacy of NAIs by way of processes such as chelation, subsite binding, statistical rebinding and aggregation.

During this project, the synthesis of two diastereomeric oseltamivir derivatives starting from shikimic acid is described. These derivatives feature a modification to the pentanol subunit in order to allow for conjugation to a multivalent scaffold using click chemistry. This research marks the first synthesis of oseltamivir derivatives where this subunit is altered with the goal of multivalent inhibition. In this project the discovery of some diastereomer-specific characteristics is also explained. These were found using both selective and non-selective decoupled NMR experiments.

1. Introduction

1.1 Influenza viruses

Influenza is an infectious respiratory disease, caused by a group of viruses that are part of the family *Orthomyxoviridae*. The group consists of seven genera, of which four contain species that cause influenza: Alpha-influenzavirus (IAV), Beta-influenzavirus (IBV), Gamma-influenzavirus (ICV) and Delta-influenzavirus (IDV)[1]. All of them are enveloped viruses with a segmented genome, which is comprised of single-stranded negative-sense RNA. Of the four types, the influenza A virus (IAV) is the biggest health concern for humans, as it has been the cause of several pandemics in the past[2–4], while presenting itself as a perpetual risk for new pandemics and epidemics[5].

There are two main reasons for the continuous threat of IAVs, namely *genetic shift* and *genetic drift*. Genetic shift is caused by the infection of a single host cell by multiple different strains of IAV and the genetic re-assortment that follows, while genetic drift occurs when RNA polymerase errors cause point mutations in the genes that encode for the antibody binding sites of the virus[6]. As both of these events lead to different genetic virus makeups, existing immunity in the host does not guarantee full protection against conceivable new strains.

The mutations that are most relevant are those of the two major surface proteins, neuraminidase (NA) and hemagglutinin (HA). Their interactions with sialic acid at the cell surface are what often initiates infection of the cell. HA enables attachment and entry by binding to sialic acid-containing receptors and infecting the cell with its RNA. Subsequently, NA causes the release of virions by cleaving off sialic acids from the receptors in order to spread the infection[7,8].

The main preventive measure against influenza is the use of vaccines. Available influenza vaccines are separable into two types: Inactivated influenza vaccines (IIV) and live attenuated influenza vaccines (LAIV). However, there are significant challenges that flu vaccines have yet to overcome, such as the uncertainty regarding reduced efficacy of vaccines when administered yearly[9] and the indication that the elderly, the group most vulnerable to the flu, benefits the least from vaccination[10].

On top of that, the aforementioned antigenic mutations also diminish the efficacy and effectiveness of vaccines, because they cannot provide immunity for all possible strains at once. Therefore, it has been common practice for countries to stockpile different vaccines specific to different strains in order to be able to pick and choose the appropriate vaccine(s) yearly[11]. One can imagine that this approach ceases to work once a variant with no readily available corresponding vaccine happens to emerge, since having to develop a new, effective vaccine and mass-produce it during the first months of a pandemic is just not viable.

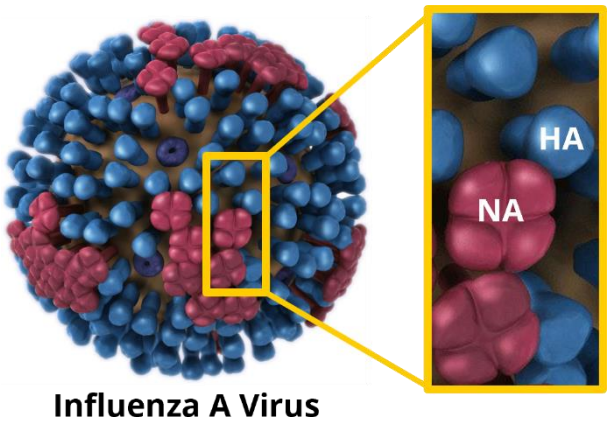

Figure 1: *Schematic representation of the Influenza A virus (IAV) and its two predominant surface proteins: Neuraminidase (NA) & Hemagglutinin (HA).*

Alternatively, the primary therapeutic measure is the use of antiviral drugs. Initially, the development of influenza antivirals focused on inhibiting the M2 protein. This is the third surface protein present on influenza virions. These M2 inhibitors are also known as the adamantanes and include amantadine and rimantadine (Figure 2a). They block the M2 proton channel, thereby preventing release of the virus ribonucleoprotein and interrupting the early stages of viral replication[7,12]. However, the M2 inhibitors do not function against IBVs and are subject to rapidly increasing drug resistance. Therefore they are no longer recommended for use[13,14].

Conversely, neuraminidase inhibitors (NAIs) have been shown to be less specific, but more effective in combating influenza. NAIs are effective against both IAV and IBV, because of the high rate of conservation of the neuraminidase active site between all subtypes[15]. These inhibitors block the NA function, preventing the release of virions. The first globally licensed NAI was zanamivir, which was developed after two important discoveries were made. The first was that sialic acid substrate 2,3-dehydro-2-deoxy-N-acetyl-neuraminic acid (DANA, Figure 2a) was a weak NA inhibitor. The second was based on a crystallographic study of NA in complex with the sialic acid substrate, where it was found that there was an empty negatively charged pocket near the C4 of the substrate ring[16]. It was then hypothesized that substituting the C4-OH with a different residue might lead to increased affinity. This led to the creation of zanamivir, where this C4-OH was replaced by a 4-guanidino group[17]. Zanamivir is administered by inhaling it as a powder.

Because of the low oral bioavailability of zanamivir, oseltamivir was developed[18]. The active compound is oseltamivir carboxylate (**OC**), but the drug is administered orally as the ethyl ester prodrug oseltamivir phosphate (**OS**, Figure 2b). It is then enzymatically converted by hepatic esterases to the active form upon absorption in the gastrointestinal tract[19]. Mainly due to its convenient administration, oseltamivir is the most used therapeutic drug.

Subsequently, peramivir was developed[20] with the idea of combining features of both zanamivir and oseltamivir. It is administered intravenously and not yet licensed globally, though it has already been approved in several countries. Finally, a fourth NAI was developed, based on tweaking the C7-OH of zanamivir by substituting it for a C7-OCH_3. Named laninamivir[21], its main advantage is that it is a long-acting NAI that is administered orally[22]. However, as of now it is only licensed in Japan.

Despite the continuing innovations regarding new antiviral influenza drugs, the overall effectiveness of the NAIs is declining. This is mostly caused by the previously mentioned mutations leading to increased resistance. Development of multivalent NAIs is one of the solutions that have been proposed to combat this problem.

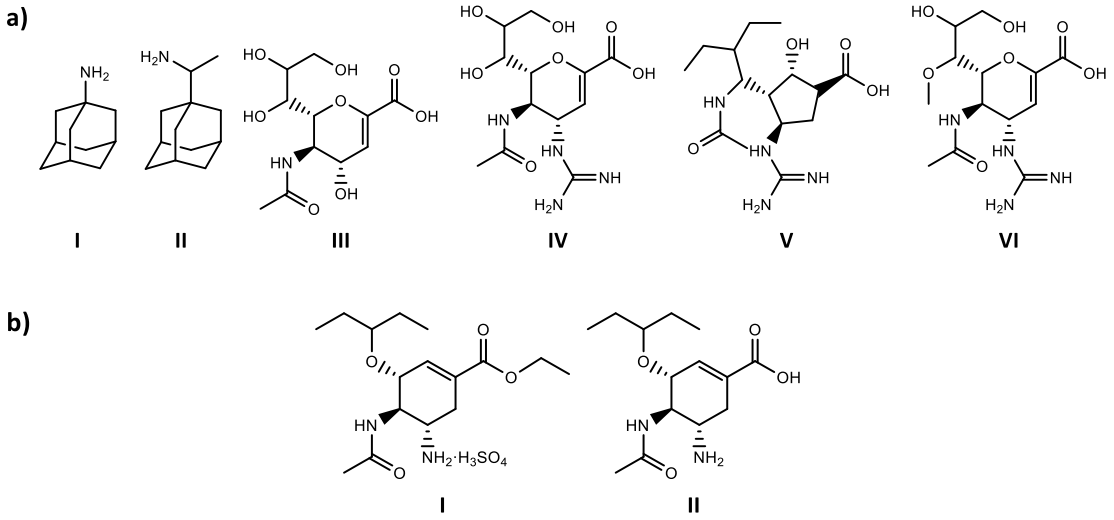

Figure 2: *Chemical structures of **a)** M2 inhibitors (I) amantadine & (II) rimantadine and NA inhibitors (III) DANA, (IV) zanamivir, (V) peramivir and (VI) laninamivir; **b)** Prodrug (I) oseltamivir phosphate (**OS**) and active compound (II) oseltamivir carboxylate (**OC**).*

1.2 Multivalency

Individual interactions between carbohydrates and proteins, such as the sialic acid-NA interaction central in influenza infections[23], are usually weak[24]. However, these individual interactions are strengthened when binding occurs at multiple sites simultaneously. This is, for example, why NA contains four binding sites. These *multivalent interactions* have been found to play a key role in biological processes such as disease progression and pathogen adhesion[25,26]. Our understanding of these complex multivalency effects has been significantly improved over the last several years, driven by a number of biochemical studies[27,28]. This has prompted an increased interest into applying the concept of multivalency to the design of inhibitors.

Multiple mechanisms can contribute to the increased potency that multivalent interactions exhibit. It is important to note that these mechanisms are not mutually exclusive and it is often impossible to quantify how much each mechanism contributes to the binding. The mechanism concerning simultaneous binding of multiple of the same ligands is known as the chelate effect (Figure 3a). A similar mechanism involving simultaneous binding of multiple different ligands is named subsite binding (Figure 3b). The improved binding potency resulting from both of these mechanisms is caused by the reduction of entropic barriers for the binding of a second ligand once a first ligand has bound[29]. The rotational and translational entropic penalties are paid by the first binding event, meaning subsequent binding events benefit from a lower entropic cost[30]. Matching binding site distances when designing multivalent ligands has been shown to be able to achieve a significant enhancement in binding affinity by utilizing this mechanism[31].

Multivalent ligands can still exhibit increased potency when only one binding site is involved in the interaction. This occurs through a mechanism named statistical rebinding[32,33] (Figure 3c). It is also possible for this mechanism to be active when the length of the multivalent ligand is not compatible with chelation. The enhancement here is caused by the slower off-rate of the ligand, since the increased local concentration of ligands around the binding site means that unbound ligands can rapidly replace released ligands due to their close proximity[30].

Intermolecular binding is also observed when researching multivalent inhibitors. This is often referred to as aggregation or crosslinking (Figure 3d). The extent to which this effect is active depends on factors like the degree of valency of the ligands, binding affinities, concentrations, conditions, etc. It is not entirely clear whether aggregation and crosslinking are a cause or a consequence of multivalency effects[30].

Several articles have reported the possibility of designing and synthesizing multivalent NAIs based on existing monovalent NAIs and examples of both are briefly discussed below. However, their outcomes do not yet show a uniform path towards understanding what specifically is necessary to make a multivalent NAI better than monovalent NAIs, further reinforcing the notion that more research is absolutely vital in order to elucidate which multivalency effects play a role at what point. Once more insight into these effects has been gained, multivalent NAI design can be optimized.

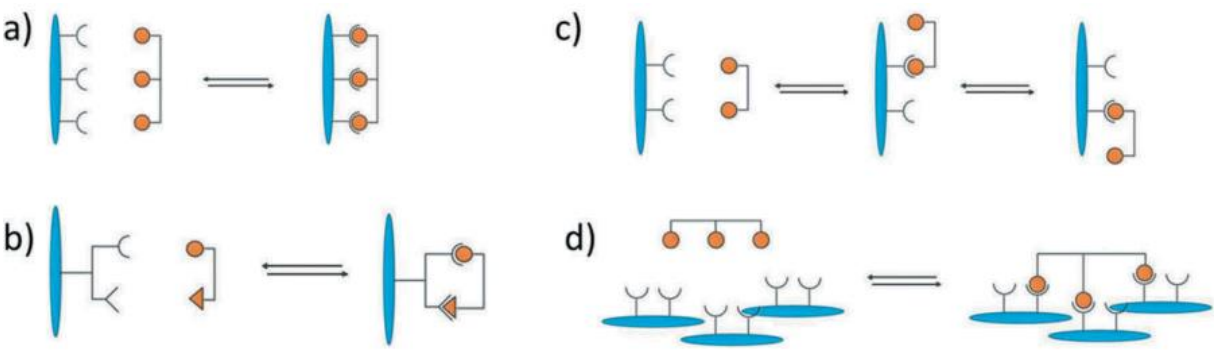

Figure 3: *Schematic representations of the different mechanisms involved in multivalent binding.* ***a)*** *Chelate effect;* ***b)*** *Subsite binding;* ***c)*** *Statistical rebinding;* ***d)*** *Aggregation/crosslinking.*[30]

1.3 Multivalent neuraminidase inhibitors

Multivalent NAIs have been a topic of interest since the crystal structure of NA showed a tetramer with four identical binding sites that displayed rotational symmetry. The distance between active sites on a single tetramer was found to be 40-50 Å. Initial attempts mainly focused on functionalizing zanamivir, after Varghese et al.[34] demonstrated that the 7-hydroxy group of zanamivir points away from the active site and is close to the protein surface when bound to influenza NA, as this is a relatively simple unit to modify.

MacDonald et al.[35] first developed a divalent zanamivir derivative using flexible linkers, ranging from 8 to 59 atoms. They found the optimal linker length to be 20 Å (Figure 4a), achieving an inhibitory potency that was approximately 100-fold higher than zanamivir. It appeared that this improvement was caused more by improved inhibition, rather than improved binding. Considering the linker length and the distance between intra-tetramer binding sites, it seems likely that mainly inter-tetramer and intervirion binding are taking place, as the linker is too short to reach multiple active sites on one tetramer simultaneously. In 2016, Fu et al.[36] took advantage of the structural knowledge of NA to synthesize a tetravalent zanamivir derivative (**TZ**, Figure 4b). Using a linker that was considerably longer, they hypothesized that this would allow **TZ** to bind to all 4 active sites of NA simultaneously (Figure 4c). However, while the crystal structure of the complex proved this to be correct and an SPR binding assay showed a 1000-fold increase in binding compared to zanamivir, **TZ** showed hardly any improvement in inhibition over monovalent zanamivir[36].

Designing multivalent **OC** has proven to be more challenging than multivalent zanamivir, mainly because there has been a collective uncertainty regarding the location of the linker, as **OC** does not contain a convenient hydroxyl handle like zanamivir. Therefore, multivalent **OC** had not been pursued until in 2019 Yan et al.[37] decided to conjugate **OC** by esterification of the carboxylic acid and elongating the ester into a linker (Figure 4d), citing “the ester prodrug masked strategy” as their inspiration for this location. Testing a variety of linker lengths, they found an optimal distance of ±32 Å between **OC** monomers, achieving a 68-fold increase in inhibition compared to the **OS** monomer. However, no comparison between the divalent **OC** analogues and monovalent **OC** was made.

It was hypothesized that this **OC** analogue would not be an improvement over monovalent **OC**, considering the x-ray structure of **OC** bound to NA[38] (Figure 5). This shows that the carboxylic acid of **OC** is involved in hydrogen bonding with NA, indicating that this unit probably contributes significantly to the potency of **OC**. Since the **OC** analogue replaces the carboxylic acid with the linker, one would expect the binding to decrease substantially.

A more suitable location for a linker appears to be the 3-pentanol unit. This unit is not involved in hydrogen bonding with NA, therefore altering it is unlikely to have a detrimental effect on the binding with NA. Based on this observation, Wei et al.[8] synthesized oseltamivir mimic (**OCM**) derivatives that were extended from the 3-pentanol unit by essentially replacing the pentanol by an alkynol spacer during the synthesis route. They then utilized click chemistry to conjugate two **OCM** derivatives to a linker that was selected based on previous success with the development of divalent galactose inhibitors[39]. From a cytopathic effect (CPE) assay it was found that while **OCM** with a spacer was a 770-fold weaker CPE inhibitor than **OC**, divalent **OCM** with a spacer length of ±40 Å (Figure 6) was a 2-fold stronger NAI than **OC**. Furthermore, it was noted that this divalent compound also exhibited some HA inhibition, which could be worth looking into more.

1.4 Aim

This project aims to design and subsequently apply a synthesis route to synthesize two diastereomeric oseltamivir derivatives. The design of the route is to be based on a combination of existing **OC** synthesis routes[40–43], while implementing a 8-nonyn-3-ol spacer instead of the usual 3-pentanol subunit, which is identical to the spacer used in the **OCM** study[8] mentioned previously. The terminal alkyne on the spacer allows for click chemistry to be used to conjugate a linker to the derivatives for the synthesis of multivalent NAIs.

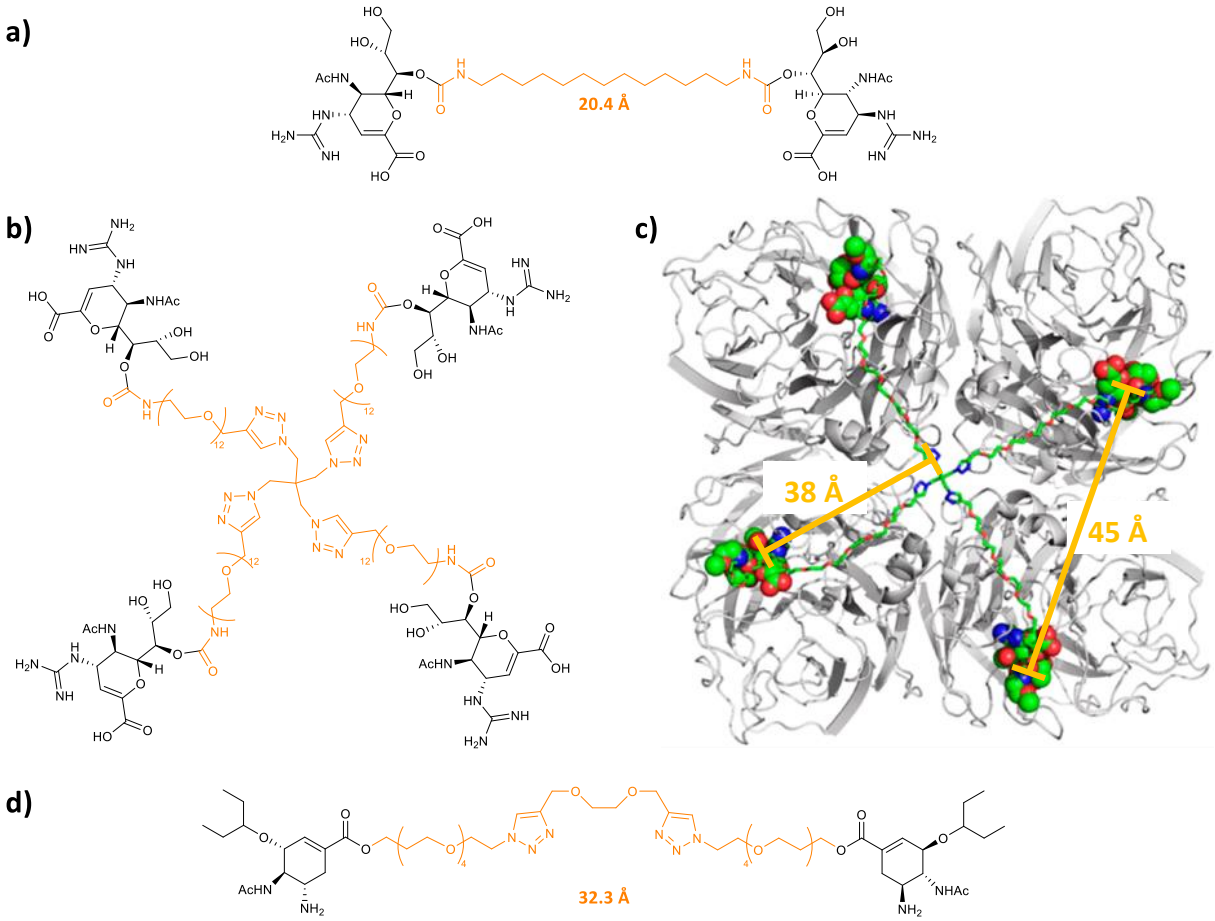

Figure 4: *Multivalent NA inhibitors.* ***a)*** *Divalent zanamivir;* ***b)*** *Tetravalent zanamivir (**TZ**);* ***c)*** *NA tetramer (PDB code 4MWX) with TZ overlay[44] ;* ***d)*** *Divalent oseltamivir carboxylate (**OC**).*

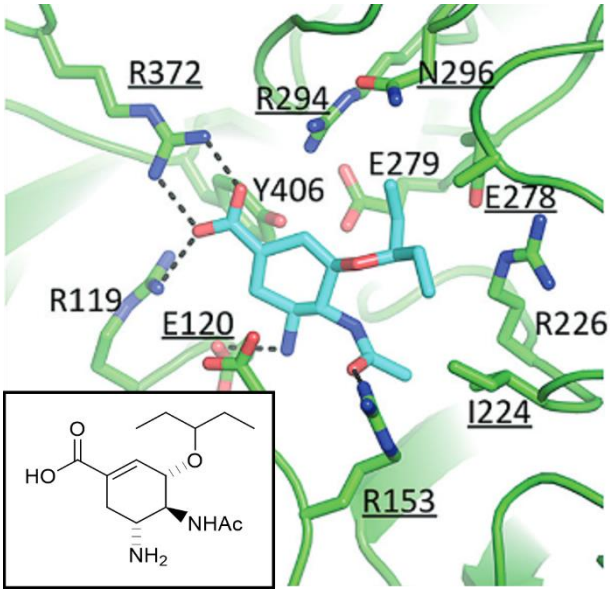

Figure 5: *X-ray structure of the NA active site with bound* ***OC*** *(PDB code 5L15)[38].*

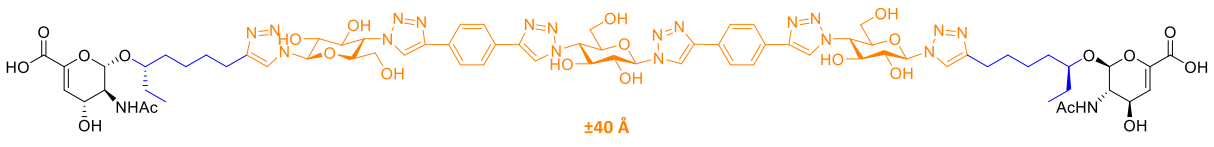

Figure 6: *Divalent oseltamivir mimic derivative where the oseltamivir mimic (**OCM**), the spacer and the linker are shown in black, blue and orange respectively.*

2. Results and discussion

2.1 Spacer synthesis

The 8-nonyn-3-ol spacer was synthesized following a protocol published by Kuang et al.[44] (Scheme 1). The first step was an alkynylation in which 1-hexyne was deprotonated by *n*-BuLi to form 1-hexynyllithium, whereupon propionaldehyde was added. This lead to the formation of 4-nonyn-3-ol (**1-rac**), which was obtained as a racemic mixture in 87% yield. Compound **1-rac** then underwent a so-called 'triple bond migration'. For this reaction, solid Li was dissolved in ethylene diamine at 80 °C forming a lithium amide salt. *t*-BuOK was then added at rt, followed 0.5 h later by **1-rac**. This yielded 8-nonyn-3-ol (**2-rac**) as a racemic mixture in 61% yield. A mechanism for this migration was proposed by Abrams and Shaw[45], which can be seen in Scheme 2. The mechanistic advantage of *t*-BuOK addition during the reaction is hypothesized by Abrams[46] to be that the potassium salt positively affects the cation exchange.

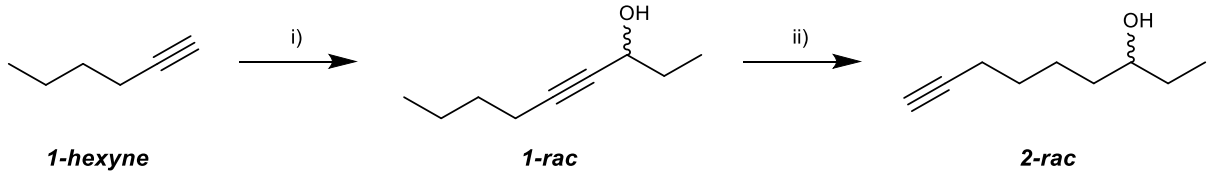

Scheme 1: *Synthesis of 8-nonyn-3-ol spacer.*
Reagents and conditions: i) *n*-BuLi (1 eq), THF, -72 °C, 1 h, then EtCHO (1 eq), -72 °C to rt, 5 h, 87%; ii) Li, *t*-BuOK (5 eq), NH_2-CH_2-CH_2-NH_2, 80 °C to rt, 18 h, 61%.

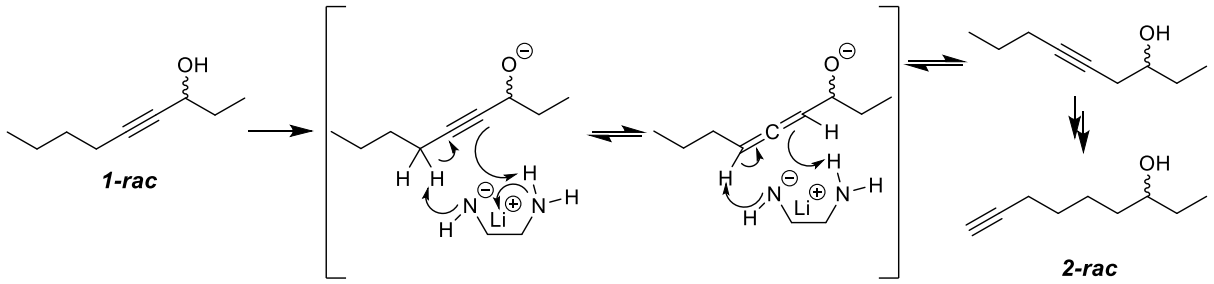

Scheme 2: *Proposed mechanism of triple bond migration[48].*

2.2 Oseltamivir derivative synthesis

Depicted in Scheme 3 is the synthesis route of the initial attempt at synthesizing the oseltamivir derivatives. The synthesis started from **(–)-shikimic acid**, since it is very common and cheap. The first step was a Fischer esterification. This reaction was first attempted with thionyl chloride in EtOH, as this was a known procedure[47] that was commonly used in **OC** syntheses, but for unknown reasons this did not lead to formation of ethyl shikimate **4** here. However, when $SOCl_2$ was replaced by Dowex H^+ resin, **(–)-shikimic acid** was quantitatively converted into compound **4**. Subsequently, compound **4** was exposed to 4.5 eq. mesyl chloride and 5 eq. triethylamine with a catalytic amount of DMAP to yield trimesylate **5** in 95% yield.

Compound **5** then underwent regioselective and stereoselective nucleophilic substitution of the OMs group at the C3 position upon addition of 4 eq. NaN_3 at 0 °C, resulting in an 88% yield of compound **6**. The stereoselective aspect of this substitution is easily explained by its S_N2 nature, whose concerted mechanism inherently features inversion. The regioselectivity can be explained by the fact that the C3 is the allylic position, so the S_N2 transition state can be stabilized by conjugation with the double bond. Therefore attack of the nucleophile on C3 is much easier than on the other two carbons.

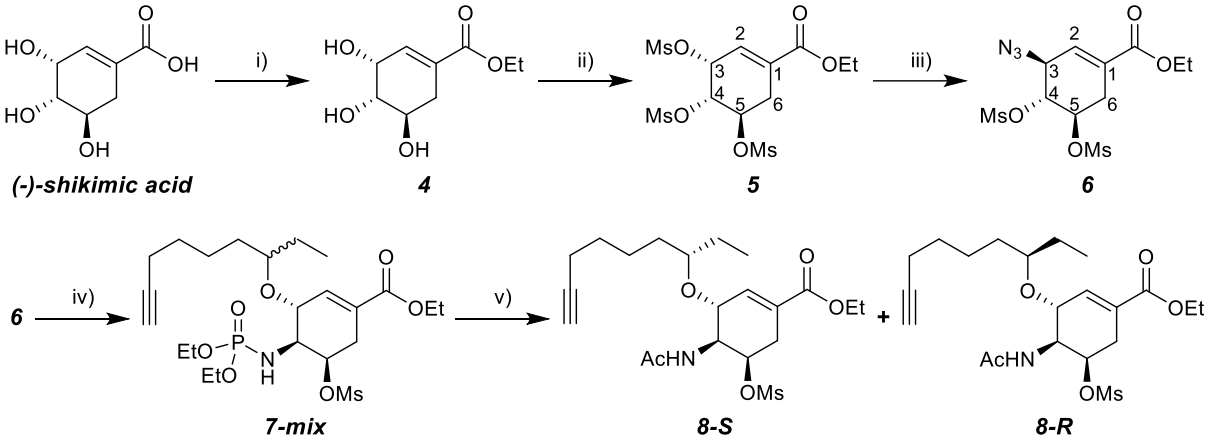

Scheme 3: Reagents and conditions: i) H^+ resin, EtOH, 85 °C, 20 h, quant.; ii) MsCl (4.5 eq), DMAP (cat.), Et_3N (5 eq), 0 °C, 2 h, 95%; iii) NaN_3 (4 eq), acetone/H_2O (5:1), 0 °C, 4 h, 88%; iv) $P(OEt)_3$ (1 eq), toluene, 120 °C, 5 h, then $BF_3{\cdot}OEt_2$ (1.2 eq), ***2-rac*** (5 eq), 0 °C to rt, 20 h, 30%; v) 96% H_2SO_4 (8 eq), EtOH, 70 °C, 20 h, then Ac_2O (1.3 eq), EtOAc, rt, 4.5 h, 43%.

Next was the introduction of alkynol spacer **2-rac** via aziridine intermediate **7-int**. The proposed mechanism of this reaction can be seen in Scheme 4. First, compound **6** was exposed to 1 eq. of $P(OEt)_3$ to produce compound **7-int**, which then underwent stereo- and regioselective Lewis acid-catalyzed ring opening with $BF_3{\cdot}OEt_2$ and compound **2-rac** to afford compound **7-mix** in 30% yield. The regioselectivity of this reaction is again explained by the fact that the allylic C3 carbon is much more reactive than the C4. The stereoselective aspect, where the (S)-configuration of the C3 carbon is inversed to the (R)-configuration upon nucleophilic attack, is caused by the fact that the alkynol must attack from the opposite side of the aziridine, due to steric hindrance and preferred cyclohexene ring arrangement among other things.

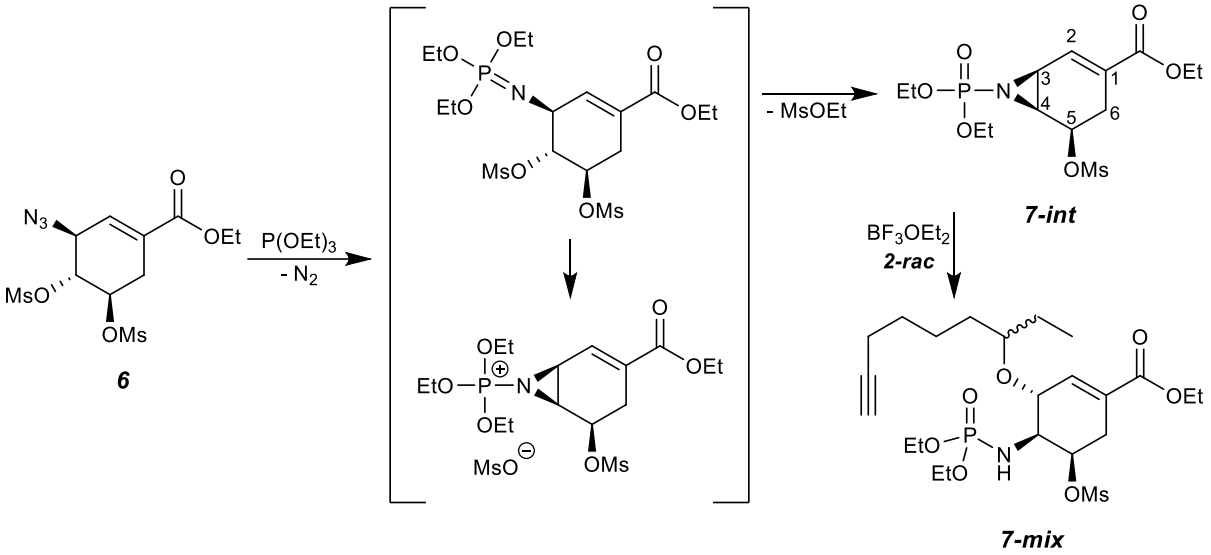

Scheme 4: *Proposed mechanism of aziridine formation*[41].

Compound **7-mix** was afforded as an inseparable mix of diastereomers. It was expected that the diastereomers would be separable after the following step once the phosphonate-group was replaced by an acetyl-group. The N-P bond was cleaved using 96% sulfuric acid, whereupon N-acetylation took place using acetic anhydride. Diastereomers **8-S** and **8-R** were indeed found to be separable using column chromatography and were collected for a combined yield of 43%. However, it was not possible to determine which of the collected products was **8-S** and which was **8-R**, just based on their different Rf values (0.4 and 0.47 in EtOAc/PE : 9/1).

Generally, one would be able to use ^1H NMR to perform these assignments, because the different diastereomers show different J-couplings between the proton on the chiral center and the protons on the neighboring carbons, depending on their conformation.

Unfortunately, this difference was not observable for these diastereomers, as can be seen in Figures S12a and S13a. It was hypothesized that this is caused by the relatively free rotation of the sidechains on the chiral center, which diminishes the effect of the difference in conformation on the J-coupling. Therefore, it was decided to revisit the spacer synthesis in order to separate the enantiomers during it, subsequently enabling the synthesis of both diastereomers individually.

2.3 Enantiospecific spacer synthesis

To facilitate the separation of spacer **2-rac** into enantiomers **2-S** and **2-R**, an enzymatic kinetic resolution was performed on racemic mixture **1-rac**. This was based on previous work by Xu et al.[48], who described how an enzyme named Novozym-435 was found to be an effective biocatalyst for the enantioselective kinetic resolution of propargylic alcohols, and Kuang et al.[44], who showed that this approach also worked for this alkynol. Novozym-435 is an immobilized lipase, whose immobilization occurs via interfacial activation of lipase B of *Candida antarctica* on an acrylic resin[49].

For this project, Novozym-435 was shown to enantioselectively acetylate the (R)-alkynol in a mixture of **1-rac** in the presence of vinyl acetate, resulting in a mixture of the (S)-alkynol **1-S** and (R)-alkynyl acetate **3** (Scheme 5). After separation via column chromatography, compound **3** was deacetylated with KOH in MeOH to afford compound **1-R** for a combined yield of 59% over the two steps. Specific optical rotation was measured to confirm the formation and separation of the two enantiomers.

Following the separation of the enantiomers, the previously described triple bond migration was performed for both enantiomers, affording compound **2-S** from compound **1-S** in 58% yield and compound **2-R** from compound **1-R** in 61% yield respectively.

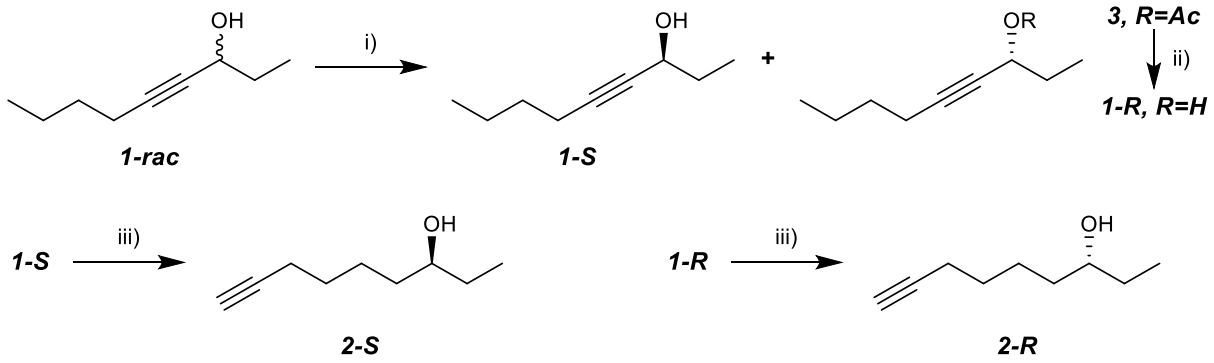

Scheme 5: *Stereospecific synthesis of 8-nonyn-3-ol spacers.*
Reagents and conditions: i) vinyl acetate, Novozym-435, 60 °C, 22 h, 60%; ii) KOH (1.1 eq), MeOH, rt, 2.5 h, 53%; iii) Li, *t*-BuOK (5 eq), NH_2-CH_2-CH_2-NH_2, 80 °C to rt, 18 h, **2-S** = 58%, **2-R** = 61%.

2.4 Synthesis and differentiation of separated oseltamivir derivative diastereomers

With the separated enantiomers of the spacers in hand, the ability to appoint the correct designation to each diastereomer was enabled once compounds **8-R** and **8-S** were synthesized again. This synthesis can be found in Scheme 6. Starting from compound **6**, compounds **7-R** and **7-S** were synthesized separately with compounds **2-R** and **2-S** respectively, according to the same protocol as earlier described. Both reactions afforded similar yields compared to the previous attempt (28% for **7-R** and 31% for **7-S** respectively). The N-P bond cleavage and the N-acetylation were also repeated, however for some unknown reason both compounds **8-R** and **8-S** were lost during the purification via column chromatography. Prior to this purification step, Rf values were obtained doing TLC of the crude products (in EtOAc/PE : 9/1: Rf = 0.39 for **8-R** and Rf = 0.47 for **8-S**). Comparing these values to those obtained, it became possible to assign which TLC spot, and therefore which fraction, corresponded to which diastereomer.

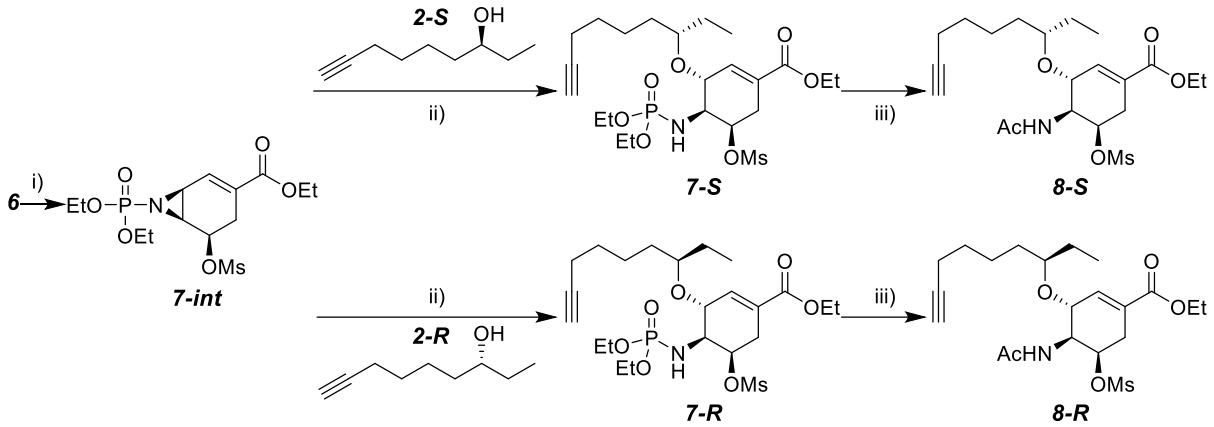

Scheme 6: Reagents and conditions: i) $P(OEt)_3$ (1 eq), toluene, 120 °C, 5 h; ii) $BF_3{\cdot}OEt_2$ (1.2 eq), 0 °C to rt, 20 h, **7-S** = 31%, **7-R** = 28%; iii) 96% H_2SO_4 (8 eq), EtOH, 70 °C, 20 h, then Ac_2O (1.3 eq), EtOAc, rt, 4.5 h, 30% (crude for both **8-S** and **8-R**).

Inspired by this result and the difficulties encountered before reaching it, the decision was made to attempt to discover more characteristic differences that can be used for future reference. Another relevant part of the reason for doing this, is that while Rf values are characteristic values for specific compounds, the two values described here are quite close to one another. It is not inconceivable that repeating this method would lead to slightly different Rf values, even when using the same eluent mixture. Therefore, several specific NMR experiments were designed in order to find more characteristics of the diastereomers, which cumulatively amount to more concrete proof when assigning either diastereomer in the future.

Based on the earlier hypothesis that the free rotation around the stereocenter causes the lack of discernible differences between NMR spectra of the two diastereomers, it was determined that a logical follow-up was to lower the temperature of the NMR sample. Temperature is correlated to the rate of rotation around a bond, where the lower the temperature, the slower the rotation. The probe of the available NMR spectrometer was only able to be cooled to 10 °C. Possibly as a result of this, differences in J-coupling were still not observed. However, discrepancies of up to 0.02 ppm were observed when comparing equivalent proton peaks of both diastereomers (Figure 8). The largest deviation was observed between H1a/H1b, the terminal proton on the alkyne, and between H7a/H7b, the proton on the stereocenter. Following these observations, it was theorized that compound **8-S** is less influenced by the shielding effect, as its peaks exhibit slightly larger chemical shifts compared to **8-R**. To lend more credence to this theory, it is recommended to repeat this experiment at a considerably lower temperature. This would increase the influence of temperature on the shielding effect, as well as possibly leading to the expected differences in J-coupling becoming visible.

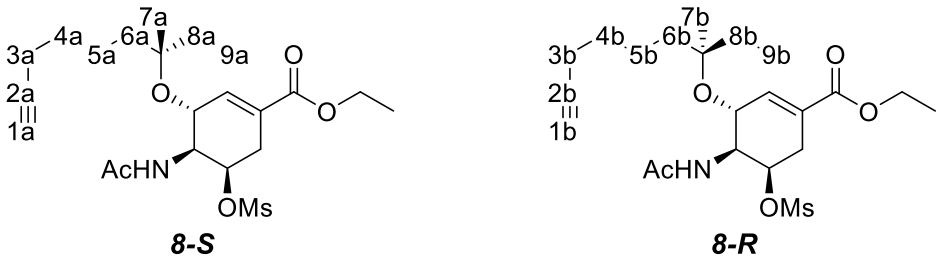

Figure 7: *Chemical structures of compounds **8-S** and **8-R** showing what each relevant atom will be referred to as during NMR characterization.*

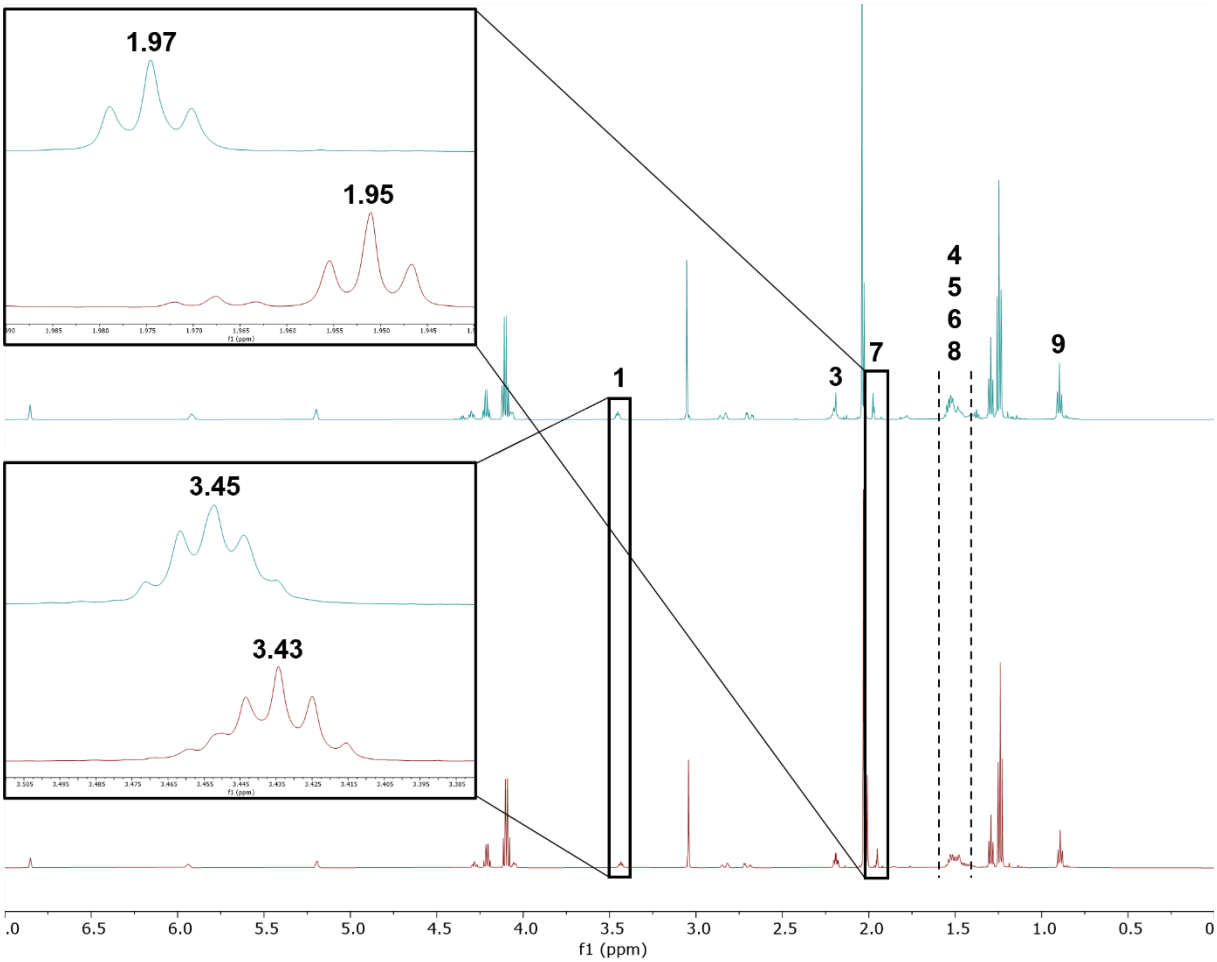

Figure 8: *^{1}H NMR spectra of **8-S** (light blue) and **8-R** (red) measured at 10°C. The highlighted parts show the difference in resonance frequency of peaks stemming from corresponding protons of both diastereomers (bottom).*

The focus was now put on the cluster of proton peaks around 1.5 ppm, because it was composed of H4, H5, H6 and H8 which are all close to the stereocenter and because it was determined there was nothing more to be gained from the other peaks. The interest was in finding out whether these individual protons did show differences based on stereochemistry, but the different parts of the cluster would have to be individually assigned to specific protons in order to find out.

Regular ^{1}H NMR could not provide the resolution necessary to separate the proton peaks, especially because of the large amounts of coupling present, which lead to very broad peaks. On top of that, HSQC was unable to help assigning C4, C5, C6 and C8. Consequently, H2BC was employed in order to solve the problem regarding the assignment of the carbons. H2BC exclusively correlates protons and non-quaternary carbons that are separated by two covalent bonds. This was particularly useful, as the correlation between the isolated proton & carbon peaks that were already assigned using HSQC and the unknown carbon peaks could be used to assign these to C4, C5, C6 and C8. This process is shown in Figure S16. Now that all the relevant carbons were assigned, the issue of the broad proton peaks was solved by utilizing so-called 'pure shift' HSQC spectroscopy.

Pure shift NMR spectroscopy removes the effects of homonuclear ^{1}H-coupling using a broadband decoupler. This method was specifically developed to disentangle overlapping peaks in ^{1}H spectra. It can be used in combination with HSQC to allow for spectra to be produced that only contain chemical shifts in both dimensions, because the proton multiplets are all collapsed into singlets. This aspect is of great importance in this particular case, since it leads to much narrower proton peaks. The results of the pure shift HSQC experiments can be seen in Figure 9.

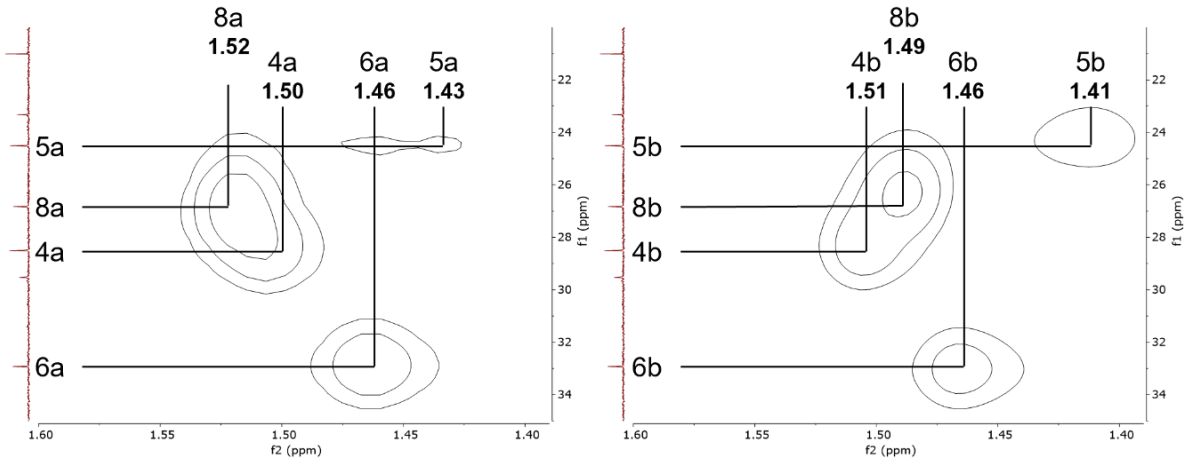

Figure 9: *Pure shift HSQC spectra of* ***8-S*** *(left) and* ***8-R*** *(right).*

Some interesting observations can be made by analyzing these spectra. Firstly, it appears that of the two freely rotating subunits connected to the stereocenter, the protons located on the one with the terminal alkyne do not seem to be influenced by the stereochemistry. H4, H5 and H6 all exhibit the same chemical shift, considering the error margin reading from a 2-dimensional spectrum. Secondly, the proton located on the other subunit does seem to be influenced by the stereochemistry, showing a difference of 0.03 ppm between H8a and H8b. It is especially important to note that there is not only a difference in chemical shift itself, but that the resonance frequency of H8 is also different relative to the other protons of the same diastereomer (i.e. the order for **8-S** is 8a-4a-6a-5a while for **8-R** it is 4b-8b-6b-5b). This indicated that manipulating the shape of one of the peaks within the cluster should express itself by appearing as a differently shaped cluster, depending on the diastereomer. This is where selective homonuclear decoupling, or HOMODEC, came in.

HOMODEC is a 1-dimensional NMR spectroscopy variant where a single resonance frequency is selectively decoupled. This means that protons that couple to the proton that corresponds to the decoupled resonance frequency lose that specific coupling, thus changing the shape of their peak. For the purposes of this research, it was concluded that H9 was most useful to be decoupled, as it meant that the shape of only H8 within the cluster of peaks would change. It is technically correct that H9 could also couple with H7 and even H6/H5, but these coupling constants would be too small to be visible at the measured resolution. It is important to keep in mind that the peak of H8 does not disappear entirely, it is merely collapsed from a multiplet into a doublet (Figure 10). The remaining multiplicity stems from the coupling of H8 with H7, which was not decoupled. ^{1}H NMR spectra where the resonance frequency corresponding to 0.90 ppm was decoupled were taken and the results of this can be seen in Figure 11.

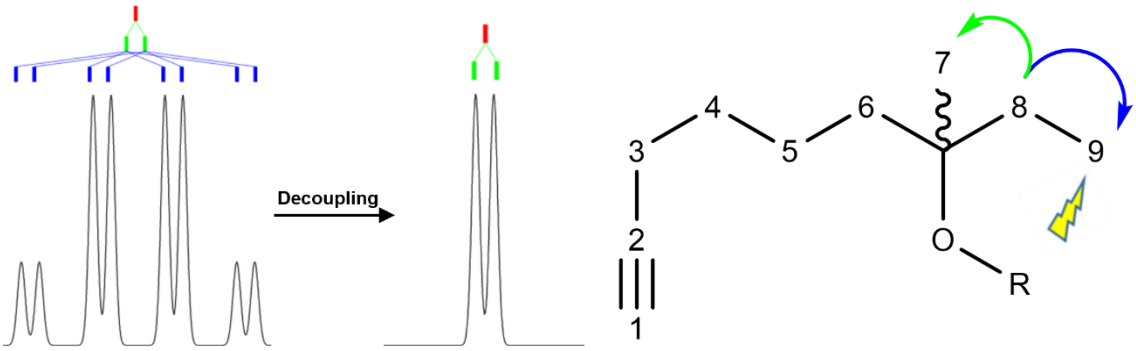

Figure 10: *Visual representation of the effect of the decoupling at 0.90 ppm on the shape of the H8 peak using approximations of the coupling constants.*

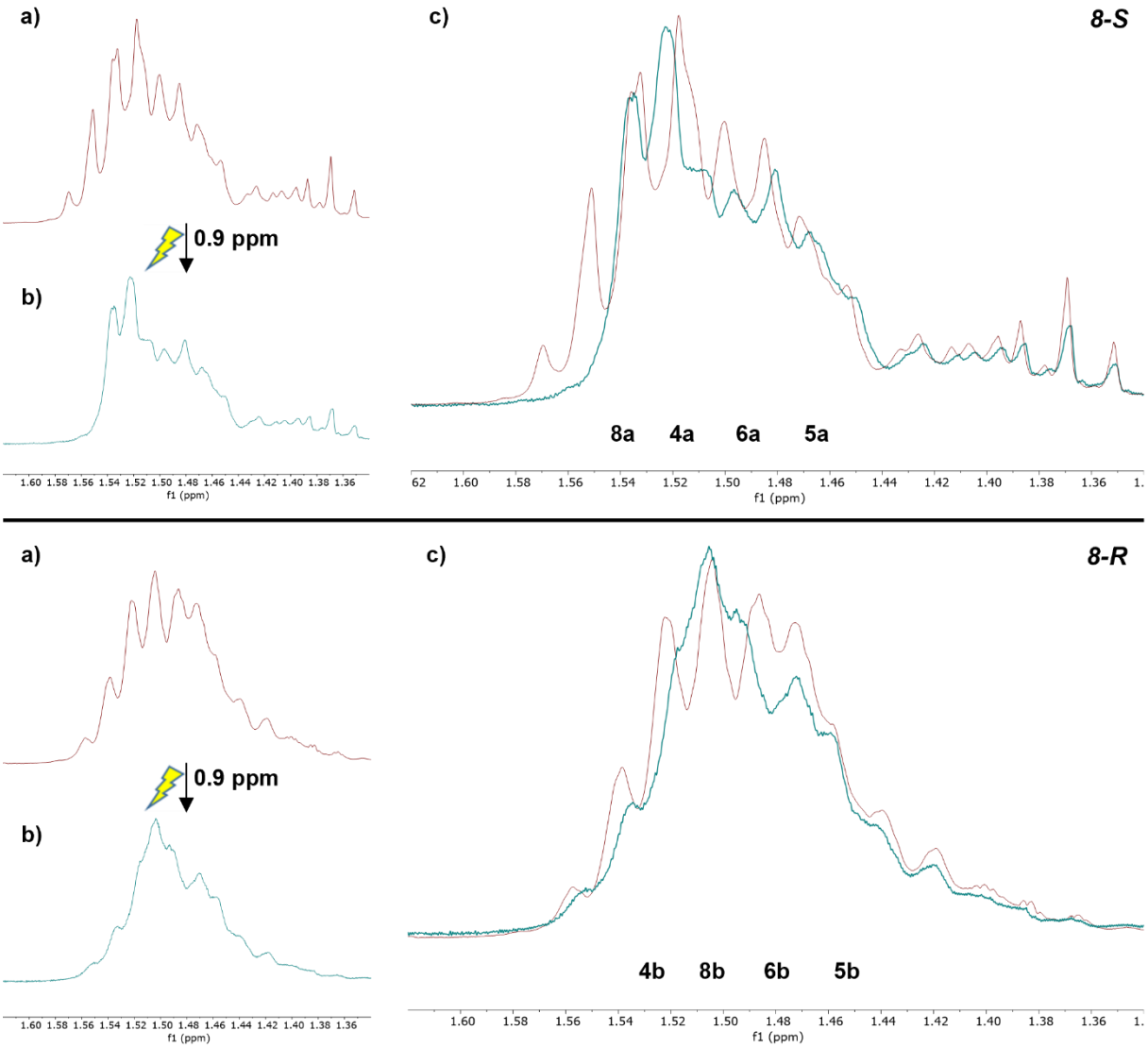

Figure 11: *Selected regions (indicated with dashed lines in Figure) of ^{1}H spectra of compounds **8-S** (top) and **8-R** (bottom); **a)** conventional ^{1}H spectra; **b)** selectively homonuclear decoupled (HOMODEC) ^{1}H spectra where the decoupled frequency is the resonance frequency of H9, which corresponds to 0.9 ppm; **c)** Overlays of the two spectra per diastereomer, showing the influence of decoupling on the surrounding protons. Also shown are the approximate locations of those proton peaks, ordered according to Figure.*

By overlaying a regular ^{1}H spectrum with its corresponding decoupled spectrum, the influence of decoupling on the shape of the peaks can be easily determined. The expectation for compound **8-S** was that the left side of the cluster would change in shape, as H8a was determined to be the proton with the highest chemical shift of the four. Conversely, for compound **8-R** the shape change was expected to more be towards the middle of the cluster, since H8b has the second highest chemical shift here and not the highest. For the **8-S** overlay, the left-most two peaks of the cluster clearly disappeared upon decoupling, while the peak intensity around the center of H8a remained constant. The peak intensity to the right of the H8a center also decreases, but is not removed entirely, as the other protons also contribute to the peak intensity of the cluster here. This is in accordance with the aforementioned expectations. For the **8-R** overlay, the differences are slightly more difficult to spot, which was unsurprising considering H8b is located more in the middle of the cluster, but deviations can still be found. Similarly to H8a, the areas to the left and right of the H8b peak center lost some intensity upon decoupling. Also, the peak center gained in intensity, which can be explained by the fact that the coupled H8 peak actually does not feature a peak at its peak center, as seen in Figure 10.

To summarize, the characteristic differences elucidated from these NMR experiments, combined with the Rf values, cumulatively provide concrete evidence that can be used to correctly assign these diastereomers in future research.

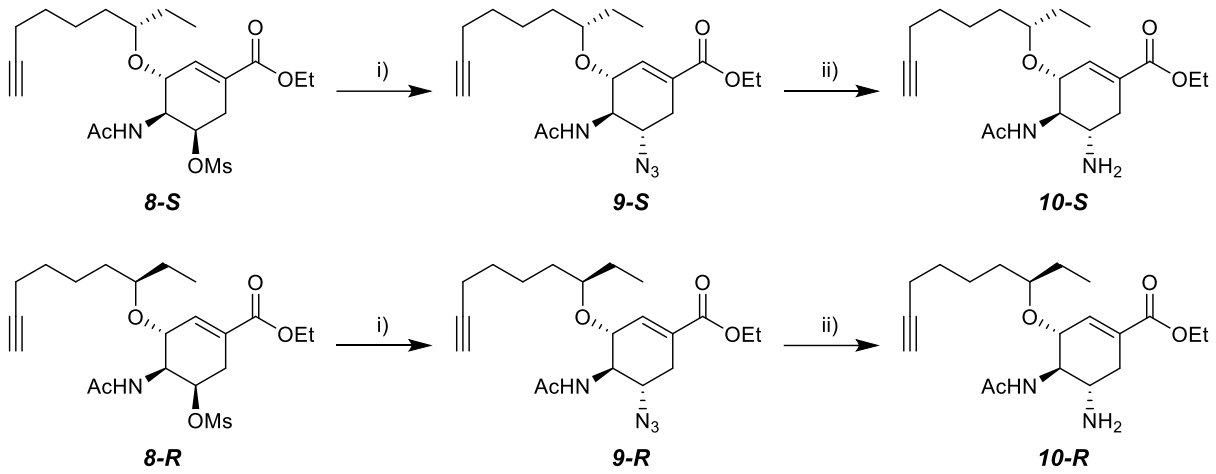

Scheme 7: Reagents and conditions: i) NaN_3 (4 eq), EtOH/H_2O (5:1), 95 °C, 20 h, 9-S = 70%, 9-R = 74%; ii) Ph_3P (1.5 eq), THF/H_2O (5:1), 45 °C, 20 h, 10-S = 38%, 10-R = 31%.

2.5 Final oseltamivir derivative synthesis

Once the extensive exploration into NMR experiments for diastereomer elucidation had concluded, the focus returned to the continuation of the synthesis of the **OC** derivatives. The remaining steps can be seen in Scheme 7. Starting from diastereomers **8-S** and **8-R**, an azide was introduced via nucleophilic substitution of the OMs-group. This was a similar reaction to the earlier introduction of an azido group on compound **5**, but this time regioselectivity did not play a role. This was reflected in the reaction conditions, which were more severe than previously. Treating compounds **8-S** and **8-R** with 4 eq. NaN_3 in EtOH/H_2O (5:1) at 95 °C for 20 h afforded compounds **9-S** and **9-R** in 70% yield and 74% yield respectively. Due to the nature of S_N2-reactions, the stereochemistry was again inverted.

The introduced azido groups were subsequently converted into amino groups. During most **OC** syntheses, this reduction is performed using hydrogen gas and Lindlar-catalyst. However, for this research this is not possible as the alkyne would also be reduced. Therefore it was decided to employ a Staudinger reduction. Compounds **9-S** and **9-R** were exposed to 1.5 eq triphenylphosphine in THF/H_2O (5:1) at 45 °C for 20 h, resulting in a 38% yield and a 31% yield for **10-S** and **10-R** respectively.

Initially, it was planned to conclude this project by saponification of the ethyl ester so that the final compounds would be the oseltamivir derivative equivalents of **OC** itself, i.e. the active version of oseltamivir. However, due to limited time, the saponification reactions were not performed, leaving the final compounds to be **10-S** and **10-R**, which are the equivalents of oseltamivir free base. A possible benefit of this decision is that it may actually be easier to perform click reactions on these ethyl ester compounds as opposed to the carboxylic acid-containing compounds, considering for example potential differences in solubility and stability. Also, saponification can still be performed after the click reactions.

3. Future prospects

Currently, this project describes the synthesis of two diastereomeric oseltamivir derivatives. The synthesis route was largely adapted from existing oseltamivir syntheses, meaning that where applicable, as little as possible was changed. This was done because the objective was to first find out whether the steps would still work at all with the derivatives, before eventually optimizing reaction conditions. Not all of these optimizations were actually performed, due to time constraints. Most importantly, the step where the spacer was introduced, the following step where the N-P bond is cleaved and the amino group is acetylated and the step containing the Staudinger reduction afforded quite low yields and were not optimized. It is therefore recommended to perform optimization studies for these reactions.

Some specific variables that should be looked at are the solvent choice during the spacer introduction and the ratio of spacer and intermediate during the same reaction, on top of the common variables such as reaction time and temperature.

The project also described several NMR experiments that were used for diastereomer elucidation. As mentioned earlier, due to technical limitations the optimal resolutions for these experiments were not reached. For the purposes of future research, these experiments should be repeated on an NMR spectrometer with more capabilities regarding cooling the probe and with a stronger magnet. The latter would not only improve the resolution of the current experiments, but could also expand the scope of the use of selective homonuclear decoupling, as its usefulness is connected to the resolution of the spectrometer. When the resolution is higher, a more specific resonance frequency can be decoupled, providing the opportunity to further dissect the cluster of proton peaks that was the subject of most of this elucidation process.

The two **OC** derivatives prepared during this research can now be used for various purposes. Testing the inhibitory potency of **9-S** and **9-R** and comparing the results to each other, as well as to the previously mentioned **OCM** derivatives, should be the initial priority for further research. In order to do this, **9-S** and **9-R** will first need to undergo saponification. In accordance to the research previously done on the **OCM** derivatives, a MUNANA assay and a MDCK CPE assay should be employed to test inhibition for accurate comparisons.

Subsequently, **9-S** and **9-R** should be conjugated to the linker used for the **OCM** derivatives so that these divalent compounds can also be tested and compared to each other. The conjugation can be done either before or after the saponification and should yield three different divalent compounds dependent on the combination of **OC** derivatives used (**9-S** + **9-S**; **9-R** + **9-R** & **9-R** + **9-S**). Again, the same assays should be employed for accurate comparisons. It could also be interesting to study possible HA inhibition of the divalent compounds using biolayer interferometry (BLI), since the divalent **OCM** compounds exhibited unforeseen HA inhibition.

Finally, the great potential of this successful synthesis of oseltamivir derivatives is the wide variety of scaffolds these derivatives can be conjugated with, which is made possible by the relatively recent meteoric rise of click chemistry. Examples of these larger multivalent scaffolds include Au nanoparticles and polymers like hyperbranched polyglycerol. Conjugating the derivatives synthesized in this project to any number of these multivalent scaffolds provides endless possibilities of future research that can be done in this field, so far dominated by monovalent NA inhibitors.

4. Conclusion

The synthesis route of two oseltamivir derivatives was designed and the two diastereomeric oseltamivir derivatives **9-S** and **9-R** were successfully synthesized. These compounds mark the first oseltamivir derivatives where the pentanol unit is altered to allow conjugation in order to facilitate the formation of multivalent NA inhibitors. Also described was the discovery of some characteristics that were found to be specific to each diastereomer with the use of both selective and non-selective decoupled NMR experiments.

5. Experimental methods

General. All chemicals were obtained from commercial sources and were used without further purification unless described otherwise. Synthesis grade solvents were used and stored under argon over 4 Å molecular sieves. TLC analysis was performed on SilicaPlate TLC Aluminum Backed TLC F254 (SiliCycle) plates. TLC spots were visualized with potassium permanganate (600 mL H_2O, 10 mL 5% aqueous NaOH, 40 g K_2CO_3 and 6 g $KMnO_4$) and UV light (254 nm). ^1H NMR and ^{13}C NMR spectra were recorded on an Agilent 400 spectrometer (300 MHz and 101 MHz) and Bruker Avance Neo 600 spectrometer (600 MHz). Chemical shifts are reported in ppm relative to TMS (0.00 ppm for ^1H NMR). Specific rotation was measured using a Jasco P-1010 polarimeter.

Synthesis of 4-nonyn-3-ol (1-rac). 1-hexyne (11.4 mL, 0.1 mol) and dry THF (100 mL) were added to a two-necked round-bottom flask under Ar atmosphere. The mixture was cooled to -70 °C with an EtOH-dry ice bath while stirring. *n*-BuLi (2.5 M in hexane; 40 mL, 0.1 mol, 1 eq) was added dropwise over 30 minutes. The resulting reaction mixture was stirred for 1 hour at -70 °C. Propionaldehyde (3.65 mL, 0.1 mol, 1 eq) was added dropwise and the reaction is left stirring for 16 hours, during which the temperature naturally raised to rt. An aqueous saturated ammonium chloride solution was then added to quench the reaction. The aqueous layer was extracted with diethyl ether (3x) and the organic layer was combined. After drying over $MgSO_4$, solvent was evaporated under reduced pressure and the remaining product was dried under high vacuum. **4-nonyn-3-ol (1-rac)** was obtained as a yellow liquid (13.18 g, 94%), which was used in the next step without further purification.
^1H NMR (400 MHz, $CDCl_3$) δ 4.25 (t, J = 6.6 Hz, 1H), 2.16 (td, J = 6.9, 1.9 Hz, 2H), 1.71 – 1.56 (m, 2H), 1.49 – 1.30 (m, 5H), 0.95 (t, J = 7.3 Hz, 3H), 0.87 (t, J = 7.1 Hz, 3H).

Kinetic resolution of 4-nonyn-3-ol (1-rac). Novozym-435 (1.002 g) and compound **1-rac** (6 g, 42.8 mmol) were added to vinyl acetate (140 mL). The mixture was stirred at 60 °C and the reaction was followed by TLC and NMR. After 22 hours, the mixture was cooled to room temperature. Filtration and evaporation under reduced pressure were performed before column chromatography (eluent: PE/EtOAc : 20/1) yielded **(S)-4-nonyn-3-ol (1-S)** (1.94 g) and **(R)-4-nonyn-3-yl acetate (3)** (4.05 g).
(S)-4-nonyn-3-ol:
$[\alpha]_D^{24.5}$ = -2.57 (c = 1.00, $CHCl_3$)
^1H NMR (400 MHz, $CDCl_3$) δ 4.31 – 4.23 (m, 1H), 2.18 (td, J = 7.1, 1.9 Hz, 2H), 1.73 – 1.60 (m, 2H), 1.51 – 1.33 (m, 5H), 0.97 (t, J = 7.4 Hz, 3H), 0.89 (t, J = 7.2 Hz, 3H).
^{13}C NMR (101 MHz, $CDCl_3$) δ 85.40, 81.04, 63.88, 31.17, 30.72, 21.85, 18.29, 13.50, 9.39.
(R)-4-nonyn-3-yl acetate:
^1H NMR (400 MHz, $CDCl_3$) δ 5.29 (tt, J = 6.4, 2.0 Hz, 1H), 2.19 (td, J = 7.0, 2.0 Hz, 2H), 2.05 (s, 3H), 1.77 – 1.69 (m, 2H), 1.51 – 1.32 (m, 4H), 0.97 (t, J = 7.4 Hz, 3H), 0.88 (t, J = 7.2 Hz, 3H).
^{13}C NMR (101 MHz, $CDCl_3$) δ 170.04, 86.17, 77.32, 65.66, 30.55, 28.32, 21.84, 21.04, 18.32, 13.50, 9.30.

Synthesis of (R)-4-nonyn-3-ol (1-R). Compound **3** (4 g, 21.95 mmol) and KOH (1.35 g, 24.14 mmol, 1.1 eq) were added to MeOH (33 mL) and stirred at room temperature for 22 hours. The mixture was acidified to pH 7 by adding H^+ Amberlite resin and then filtrated. Solvent evaporation under reduced pressure was performed before dissolving the remaining solid in Et_2O. This mixture was washed with H_2O and dried over Na_2SO_4. Evaporation under reduced pressure was performed and the remaining product was dried under high vacuum. **(R)-4-nonyn-3-ol (1-R)** (1.632 g, 53%) was obtained as a yellow liquid.
$[\alpha]_D^{24.5}$ = +2.23 (c = 1.01, $CHCl_3$)
^1H NMR (400 MHz, $CDCl_3$) δ 4.28 (tt, J = 6.4, 2.0 Hz, 1H), 2.19 (td, J = 7.0, 2.0 Hz, 2H), 1.75 – 1.59 (m, 2H), 1.51 – 1.33 (m, 5H), 0.98 (t, J = 7.4 Hz, 3H), 0.89 (t, J = 7.2 Hz, 3H).

General procedure of synthesis of 8-nonyn-3-ol (2-rac). Solid Li (±12 eq) was cut into small pieces and added to 1,2-diaminoethane under Ar atmosphere at room temperature. The suspension was slowly heated to 80 °C and kept stirring at that temperature until all Li was dissolved (±24 hours). The mixture was then cooled down and *t*-BuOK (5 eq) was added at rt. After 45 minutes of stirring, compound **1** was added and the reaction mixture was stirred for 2 hours. The reaction was quenched by slowly adding cold water to the mixture before transferring it to a separation funnel. The aqueous layer was extracted with diethyl ether (3x) and the organic layer was combined. The combined layer was washed consecutively with 1 N HCl and a saturated aqueous $NaHCO_3$ solution, then dried over Na_2SO_4. Filtration and evaporation under reduced pressure were performed before column chromatography (eluent: PE/Et_2O : 7/3) yielded 8-nonyn-3-ol as a yellow liquid.

For (R)-8-nonyn-3-ol (2-R): Following the procedure above, the reaction of 1,2-diaminoethane (40 mL), Li (0.5 g), *t*-BuOK (3.6 g, 32.09 mmol) and compound **1-R** (0.9 g, 6.42 mmol) afforded compound **2-R** (556 mg, 61.8%) as a yellow liquid.

^{1}H NMR (400 MHz, CDCl3) δ 3.55 – 3.47 (m, 1H), 2.18 (tdt, J = 6.4, 2.8, 1.9 Hz, 2H), 1.92 (td, J = 2.8, 0.6 Hz, 1H), 1.62 – 1.33 (m, 9H), 0.91 (td, J = 7.5, 2.5 Hz, 3H).

^{13}C NMR (101 MHz, cdcl3) δ 84.45, 72.99, 68.25, 36.29, 30.11, 28.44, 24.76, 18.33, 9.82.

For (S)-8-nonyn-3-ol (2-S): Following the procedure above, the reaction of 1,2-diaminoethane (40 mL), Li (0.5 g), t-BuOK (3.0 g, 26.74 mmol) and compound **1-S** (0.75 g, 5.35 mmol) afforded compound **2-S** (437 mg, 58.3%) as a yellow liquid.

^{1}H NMR (400 MHz, $CDCl_3$) δ 3.57 – 3.47 (m, 1H), 2.19 (tdt, J = 5.7, 2.7, 1.4 Hz, 2H), 1.93 (tt, J = 2.7, 0.8 Hz, 1H), 1.61 – 1.35 (m, 9H), 0.92 (td, J = 7.4, 1.1 Hz, 3H).

^{13}C NMR (101 MHz, $CDCl_3$) δ 84.46, 73.03, 68.25, 36.31, 30.13, 28.45, 24.77, 18.35, 9.83.

Synthesis of ethyl (3R,4S,5R)-3,4,5-trihydroxycyclohex-1-ene-1-carboxylate (4). Shikimic acid (5 g, 28.7 mmol) was dissolved in 20 mL EtOH under Ar atmosphere. Amberlite H^+ resin (10 g) was added and the mixture was heated to 85 °C. After 16 hours of reflux the mixture was cooled to room temperature. The resin was then filtered off and the EtOH was evaporated under reduced pressure, followed by drying under high vacuum. Compound **4** was obtained as a white powder (5.8 g, 100%), which was used in the next step without further purification.

^{1}H NMR (400 MHz, CD_3OD) δ 6.79 (dt, J = 3.7, 1.8 Hz, 1H), 4.37 (ddt, J = 4.1, 3.7, 1.9 Hz, 1H), 4.20 (q, J = 7.1 Hz, 2H), 3.99 (dt, J = 7.3, 5.2 Hz, 1H), 3.69 (dd, J = 7.3, 4.2 Hz, 1H), 2.69 (dddd, J = 18.2, 4.9, 1.9, 1.8 Hz, 1H), 2.20 (dddd, J = 18.2, 5.5, 1.9, 1.8 Hz, 1H), 1.29 (t, J = 7.1 Hz, 3H).

Synthesis of ethyl (3R,4S,5R)-3,4,5-tris((methylsulfonyl)oxy)cyclohex-1-ene-1-carboxylate (5). Compound **4** (5.8 g, 28.7 mmol) was dissolved in dry EtOAc (100 mL) under Ar atmosphere, treated with MsCl (10 mL, 129 mmol, 4.5 eq) and immediately cooled to 0 °C. DMAP (1.05 g, 0.3 eq/cat.) was added, followed by dropwise addition of Et_3N (20 mL, 143.6 mmol, 5 eq). The mixture was stirred for 1.25 h at 0 °C, at which point TLC confirmed full conversion. The reaction was quenched with 1 M HCl (60 mL) and transferred to a separation funnel. The organic layer was separated and washed with 5% K_2CO_3-solution (3 x 30 mL) until the pH of the organic layer was 8-9. The organic layer was then dried over Na_2SO_4, then filtration and solvent evaporation under reduced pressure were performed. Following drying under high vacuum, compound **5** was obtained as a brown/yellow oil (12 g, 95%), which was used in the next step without further purification.

^{1}H NMR (400 MHz, $CDCl_3$) δ 6.77 (dt, J = 4.8, 2.4 Hz, 1H), 5.46 (t, J = 4.4 Hz, 1H), 5.06 (ddd, J = 9.1, 7.1, 5.9 Hz, 1H), 4.95 (dd, J = 9.2, 4.0 Hz, 1H), 4.19 (q, J = 7.2 Hz, 2H), 3.17 (ddd, J = 18.6, 5.9, 2.3 Hz, 1H), 3.14 (s, 3H), 3.13 (s, 3H), 3.09 (s, 3H), 2.64 (ddd, J = 18.6, 7.1, 2.3 Hz, 1H), 1.26 (t, J = 7.1 Hz, 3H).

Synthesis of ethyl (3S,4R,5R)-3-azido-4,5-bis((methylsulfonyl)oxy)cyclohex-1-ene-1-carboxylate (6). Compound **5** (12 g, 27.49 mmol) was dissolved in acetone (100 mL) under Ar atmosphere and cooled down to 0 °C. NaN_3 (7.2 g, 110 mmol, 4 eq) was dissolved in 20 mL H_2O. The NaN_3 solution was dropwise added to the solution of compound **5**. The mixture was stirred at 0-5 °C for 3.5 h, when TLC showed that no compound **5** was remaining. The reaction was quenched by adding toluene (100 mL) and H_2O (20 mL) and the mixture was transferred to a separation funnel. The organic layer was separated and washed with H_2O (3 x 20 mL) and brine (1 x 15 mL), then dried over $MgSO_4$. The solvent was then evaporated under reduced pressure and further toluene was removed by drying under high vacuum. Compound **6** was obtained as thick brown oil (9.28 g, 88%), which was used in the next step without further purification.

^{1}H NMR (400 MHz, $CDCl_3$) δ 6.76 (t, J = 2.7 Hz, 1H), 4.89 (td, J = 9.7, 6.1 Hz, 1H), 4.77 (dd, J = 10.0, 8.0 Hz, 1H), 4.35 – 4.29 (m, 1H), 4.26 (q, J = 7.0 Hz, 2H), 3.22 (s, 3H), 3.27 – 3.18 (m, 1H), 3.16 (d, J = 0.5 Hz, 3H), 2.68 (ddt, J = 18.1, 9.3, 3.2 Hz, 1H), 1.32 (t, J = 7.1 Hz, 3H).

General procedure of synthesis of ethyl ((3R,4S,5R)-4-((diethoxyphosphoryl)amino)-5-((methylsulfonyl)oxy)-3-(non-8-yn-3-yloxy)cyclohex-1-ene-carboxylate (7). Compound **6** was dissolved in dry toluene under Ar atmosphere. $P(OEt_3)$ (1 eq) was added at rt while stirring. After 30 minutes the reaction mixture was heated to 120 °C. After 4 hours of reflux the reaction mixture was cooled to rt. Compound **2** (5 eq) was added at rt and the mixture was cooled down to 0 °C, then $BF_3{\cdot}OEt_2$ (1.2 eq) was added and the reaction is left to warm back up to rt over 16 hours. Solvent is evaporated under reduced pressure, then the mixture is diluted with EtOAc and washed with H_2O (3x). After drying over $MgSO_4$, evaporating solvent under reduced pressure and drying under high vacuum, the compound **7** was purified using column chromatography (eluent: EtOAc/PE = 4/1) as a yellow oil.

For 7-mix: Following the procedure above, the reaction of compound **6** (0.63 g, 1.64 mmol), $P(OEt_3)$ (0.28 mL, 1.64 mmol), compound **2-rac** (1.15 g, 8.22 mmol) and $BF_3{\cdot}OEt_2$ (0.24 mL, 1.97 mmol) in 4.65 mL dry toluene, washed with 3 x 5 mL H_2O, afforded an inseparable mixture of diastereomers **7-R** and **7-S (7-mix)** (343 mg, 39%) as a yellow oil.

^{1}H NMR (400 MHz, $CDCl_3$) δ 6.83 (dt, J = 3.4, 1.9 Hz, 1H), 5.09 (dt, J = 5.1, 2.6 Hz, 1H), 4.21 (q, J = 7.0 Hz, 2H), 4.16 – 4.05 (m, 4H), 4.03 (td, J = 3.8, 1.8 Hz, 1H), 3.52 (tdd, J = 9.1, 4.7, 2.7 Hz, 1H), 3.45 (p, J = 5.2 Hz, 1H), 3.09 (s, 3H), 2.99 (t, J = 9.6 Hz, 1H), 2.82 (ddt, J = 18.8, 5.0, 2.0 Hz, 1H), 2.70 (ddt, J = 18.9, 6.4, 1.4 Hz, 1H), 2.19 (td, J = 7.5, 2.6 Hz, 2H), 1.94 (t, J = 2.6 Hz, 1H), 1.62 – 1.41 (m, 8H), 1.35 – 1.27 (m, 9H), 0.92 (t, J = 7.5 Hz, 3H).

^{13}C NMR (101 MHz, $CDCl_3$) δ 165.49, 135.08, 128.61, 84.24, 80.12, 77.65, 73.65, 68.41, 62.83, 62.74, 61.16, 53.55, 38.43, 33.04, 28.73, 28.50, 26.30, 24.16, 18.29, 16.20, 16.13, 14.16, 9.62.

For compound 7-R: Following the procedure above, the reaction of compound **6** (0.25 g, 0.65 mmol), $P(OEt_3)$ (0.11 mL, 0.65 mmol), compound **2-R** (0.457 g, 3.26 mmol) and $BF_3{\cdot}OEt_2$ (0.12 mL, 1.30 mmol) in 1.85 mL dry toluene, washed with 3 x 2 mL H_2O, afforded compound **7-R** (95 mg, 27.1%) as a yellow oil.

For compound 7-S: Following the procedure above, the reaction of compound **6** (0.20 g, 0.52 mmol), $P(OEt_3)$ (0.09 mL, 0.52 mmol), compound **2-S** (0.366 g, 2.61 mmol) and $BF_3{\cdot}OEt_2$ (0.10 mL, 0.78 mmol) in 1.5 mL dry toluene, washed with 3 x 2 mL H_2O, afforded compound **7-S** (81 mg, 31.4%) as a yellow oil.

General procedure of synthesis of ethyl (3R,4R,5R)-4-acetamido-5-((methylsulfonyl)oxy)-3-(non-8-yn-3-yloxy)cyclohex-1-ene-1-carboxylate (8). Compound **7** was dissolved in EtOH under Ar atmosphere. 96% H_2SO_4 (8 eq) was added at rt while stirring. The mixture was heated to 70 °C for 20 hours and subsequently cooled down to rt. The reaction mixture was diluted by adding EtOAc and H_2O followed by 9M NaOH (14 eq) and Ac_2O (1.15 eq) addition. After 1 hour an additional portion of Ac_2O (0.15 eq) was added and the reaction was left to stir at rt for 3.5 hours.

The mixture was transferred to a separation funnel where the organic phase was separated and the aqueous phase was extracted with EtOAc (3x). The organic phases were combined, dried over $MgSO_4$ and solvent was evaporated under reduced pressure.

For compound 8-R: Following the procedure above, the reactions of compound **7-R** (95 mg, 0.18 mmol) with 96% H_2SO_4 (0.08 mL, 1.41 mmol) in 0.5 mL EtOH and with Ac_2O (0.023 mL, 0.228 mmol) in 9M NaOH (0.27 mL, 2.47 mmol), 0.4 mL EtOAc and 0.55 mL H_2O afforded crude compound **8-R** (Rf in EtOAc/PE = 9/1 is 0.39).

For compound 8-S: Following the procedure above, the reactions of compound **7-S** (81 mg, 0.15 mmol) with 96% H_2SO_4 (0.067 mL, 1.21 mmol) in 0.4 mL EtOH and with Ac_2O (0.018 mL, 0.194 mmol) in 9M NaOH (0.23 mL, 2.11 mmol), 0.35 mL EtOAc and 0.5 mL H_2O afforded crude compound **8-S** (Rf in EtOAc/PE = 9/1 is 0.47).

For mixture of 8-R and 8-S: Following the procedure above, the reactions of the mixture **7-Mix** (525 mg, 0.98 mmol) with 96% H_2SO_4 (0.43 mL, 7.81 mmol) in 2.5 mL EtOH and with Ac_2O (0.119 mL, 1.26 mmol) in 9M NaOH (1.51 mL, 13.67 mmol), 2.3 mL EtOAc and 3.1 mL H_2O afforded a crude mix of compounds **8-R** and **8-S**. Column chromatography (eluent: EtOAc/PE = 7/1) yielded **8-R** (95 mg) and **8-S** (77 mg) for a total yield of 43.4%.

Compound 8-R:

^{1}H NMR (600 MHz, $CDCl_3$) δ 6.87 – 6.84 (m, 1H), 5.97 – 5.91 (m, 1H), 5.22 – 5.16 (m, 1H), 4.28 (td, J = 8.0, 2.5 Hz, 1H), 4.21 (q, J = 7.1 Hz, 2H), 4.07 – 4.03 (m, 1H), 3.43 (p, J = 5.6 Hz, 1H), 3.04 (s, 3H), 2.83 (dp, J = 19.1, 2.2 Hz, 1H), 2.70 (ddt, J = 19.1, 4.5, 1.5 Hz, 1H), 2.19 (td, J = 7.0, 2.7 Hz, 2H), 2.01 (s, 3H), 1.95 (t, J = 2.6 Hz, 1H), 1.57 – 1.39 (m, 8H), 1.29 (t, J = 7.2 Hz, 3H), 0.89 (t, J = 7.4 Hz, 3H).

^{13}C NMR (101 MHz, $CDCl_3$) δ 170.54, 165.60, 136.61, 127.65, 84.29, 80.71, 77.83, 72.46, 68.39, 61.17, 51.50, 38.58, 33.10, 29.61, 28.51, 26.31, 24.20, 23.27, 18.31, 14.15, 9.35.

Compound 8-S:

^{1}H NMR (600 MHz, $CDCl_3$) δ 6.87 – 6.83 (m, 1H), 5.92 (t, J = 7.5 Hz, 1H), 5.20 (td, J = 4.5, 2.4 Hz, 1H), 4.30 (td, J = 8.0, 2.4 Hz, 1H), 4.21 (q, J = 7.1 Hz, 2H), 4.07 (dd, J = 7.6, 1.7 Hz, 1H), 3.45 (p, J = 5.6 Hz, 1H), 3.05 (s, 3H), 2.84 (dp, J = 19.0, 2.2 Hz, 1H), 2.69 (ddt, J = 19.2, 4.6, 1.4 Hz, 1H), 2.20 (dtd, J = 7.1, 7.0, 2.6 Hz, 2H), 2.03 (s, 3H), 1.97 (t, J = 2.6 Hz, 1H), 1.58 – 1.44 (m, 8H), 1.29 (t, J = 7.1 Hz, 3H), 0.90 (t, J = 7.4 Hz, 3H).

^{13}C NMR (101 MHz, $CDCl_3$) δ 170.55, 165.61, 136.74, 127.69, 84.47, 81.15, 77.70, 72.61, 68.53, 61.19, 51.53, 38.66, 32.93, 29.53, 28.50, 26.83, 24.51, 23.33, 18.31, 14.16, 9.27.

Synthesis of ethyl (3R,4R,5S)-4-acetamido-5-azido-3-(((R)-non-8-yn-3-yl)oxy)cyclohex-1-ene-1-carboxylate (9-R). Compound **8-R** (230 mg, 0.518 mmol) was dissolved in 2.3 mL EtOH under Ar atmosphere. NaN_3 (135 mg, 2.07 mmol, 4 eq) was dissolved in 0.5 mL H_2O and added at rt. The mixture was heated to reflux for 16 hours, when TLC showed complete consumption of starting material. EtOH was evaporated under reduced pressure, the resulting mixture was diluted with EtOAc and H_2O and transferred to a separation funnel. The organic phase was separated, washed with brine (3x) and dried over $MgSO_4$. The solvent was then evaporated under reduced pressure and the product was dried under high vacuum. Compound **9-R** was obtained as thick brown oil (149 mg, 74%), which was used in the next step without further purification.

^{1}H NMR (400 MHz, $CDCl_3$) δ 6.78 (t, J = 2.4 Hz, 1H), 5.71 (d, J = 7.3 Hz, 1H), 4.61 (d, J = 8.8 Hz, 1H), 4.34 (td, J = 10.5, 5.7 Hz, 1H), 4.22 (q, J = 7.6 Hz, 2H), 3.45 – 3.39 (m, 1H), 3.31 – 3.20 (m, 1H), 2.87 (dd, J = 17.2, 6.6 Hz, 1H), 2.29 – 2.23 (m, 1H), 2.21 (dt, J = 7.0, 2.8 Hz, 2H), 2.03 (s, 3H), 1.95 (td, J = 5.0, 2.4 Hz, 1H), 1.60 – 1.43 (m, 8H), 1.32 – 1.27 (m, 3H), 0.90 (t, J = 7.5 Hz, 3H).

^{13}C NMR (101 MHz, $CDCl_3$) δ 171.50, 166.37, 138.09, 80.74, 73.58, 68.84, 61.53, 58.78, 57.44, 33.54, 31.03, 29.05, 26.42, 24.91, 24.07, 18.82, 14.66, 9.70.

Synthesis of ethyl (3R,4R,5S)-4-acetamido-5-azido-3-(((S)-non-8-yn-3-yl)oxy)cyclohex-1-ene-1-carboxylate (9-S). Compound **8-S** (240 mg, 0.541 mmol) was dissolved in 2.4 mL EtOH under Ar atmosphere. NaN_3 (140.7 mg, 2.16 mmol, 4 eq) was dissolved in 0.5 mL H_2O and added at rt. The mixture was heated to reflux for 16 hours, when TLC showed complete consumption of starting material. EtOH was evaporated under reduced pressure, the resulting mixture was diluted with EtOAc and H_2O and transferred to a separation funnel. The organic phase was separated, washed with brine (3x) and dried over $MgSO_4$. The solvent was then evaporated under reduced pressure and the product was dried under high vacuum. Compound **9-S** was obtained as thick brown oil (147 mg, 70%), which was used in the next step without further purification.
^{1}H NMR (400 MHz, $CDCl_3$) δ 6.77 (t, J = 2.5 Hz, 1H), 5.84 (d, J = 7.4 Hz, 1H), 4.64 (d, J = 9.0 Hz, 1H), 4.36 – 4.31 (m, 1H), 4.21 (q, J = 7.3 Hz, 2H), 3.40 (t, J = 5.5 Hz, 1H), 3.25 (ddd, J = 11.2, 9.1, 8.1 Hz, 1H), 2.86 (dd, J = 17.6, 5.7 Hz, 1H), 2.30 – 2.24 (m, 1H), 2.22 (dt, J = 8.6, 2.7 Hz, 2H), 2.04 (s, 3H), 1.98 (t, J = 2.6 Hz, 1H), 1.58 – 1.44 (m, 8H), 1.29 (t, J = 7.1 Hz, 3H), 0.91 (t, J = 7.4 Hz, 3H).
^{13}C NMR (101 MHz, $CDCl_3$) δ 171.20, 138.19, 128.37, 81.36, 73.54, 68.72, 61.21, 58.73, 57.06, 32.98, 30.65, 28.54, 27.08, 24.62, 23.81, 18.58, 14.34, 9.53.

Synthesis of ethyl (3R,4R,5S)-4-acetamido-5-amino-3-(((R)-non-yn-3-yl)oxy)cyclohex-1-ene-1-carboxylate (10-R). Compound **9-R** (100 mg, 0.256 mmol) was dissolved in 3 mL THF under Ar atmosphere. Ph_3P (101 mg, 0.384 mmol, 1.5 eq) and 0.56 mL H_2O were added at rt. The mixture was heated to 45-50 °C for 20 hours, after which the THF was evaporated under reduced pressure. The residue was then partitioned between EtOAc and brine and the organic phase was separated, dried over $MgSO_4$ and the solvent was evaporated under reduced pressure to yield compound **10-R** (Rf in EtOAc/MeOH = 2/1 is 0.30). Column chromatography (eluent: EtOAc/MeOH : 2/1 to 1.5/1) yielded compound **10-R** (29 mg, 31.1%) as a yellow/brown sticky solid.
^{1}H NMR (400 MHz, $CDCl_3$) δ 6.77 (t, J = 2.2 Hz, 1H), 5.76 (d, J = 8.1 Hz, 1H), 4.26 – 4.16 (m, 3H), 3.53 (td, J = 10.1, 8.6 Hz, 1H), 3.44 – 3.37 (m, 1H), 3.24 (td, J = 10.1, 5.3 Hz, 1H), 2.80 – 2.67 (m, 1H), 2.20 (td, J = 6.9, 2.6 Hz, 2H), 2.16 – 2.09 (m, 1H), 2.03 (s, 3H), 1.95 (t, J = 2.7 Hz, 1H), 1.58 – 1.40 (m, 8H), 1.27 (t, J = 7.2 Hz, 3H), 0.88 (t, J = 7.3 Hz, 3H).
^{13}C NMR (101 MHz, $CDCl_3$) δ 171.00, 166.24, 137.34, 84.39, 80.04, 74.71, 68.33, 60.86, 58.74, 49.02, 33.50, 33.03, 28.57, 26.06, 24.39, 23.64, 18.34, 14.18, 9.21.

Synthesis of ethyl (3R,4R,5S)-4-acetamido-5-amino-3-(((S)-non-yn-3-yl)oxy)cyclohex-1-ene-1-carboxylate (10-S). Compound **9-S** (115 mg, 0.295 mmol) was dissolved in 3.45 mL THF under Ar atmosphere. Ph_3P (116 mg, 0.442 mmol, 1.5 eq) and 0.65 mL H_2O were added at rt. The mixture was heated to 45-50 °C for 20 hours, after which the THF was evaporated under reduced pressure. The residue was then partitioned between EtOAc (10 mL) and brine (5 mL) and the organic phase was separated, dried over $MgSO_4$ and the solvent was evaporated under reduced pressure to yield crude compound **10-S** (Rf in EtOAc/MeOH = 2/1 is 0.42). Column chromatography (eluent: EtOAc/MeOH : 2/1 to 1.5/1) yielded compound **10-S** (41 mg, 38.1%) as a yellow/brown sticky solid.
^{1}H NMR (400 MHz, $CDCl_3$) δ 6.78 (t, J = 2.1 Hz, 1H), 5.53 (d, J = 8.1 Hz, 1H), 4.26 – 4.16 (m, 3H), 3.50 (dt, J = 10.3, 8.2 Hz, 1H), 3.41 (t, J = 5.4 Hz, 1H), 3.26 (td, J = 9.9, 5.3 Hz, 1H), 2.74 (dd, J = 17.8, 5.4 Hz, 1H), 2.25 – 2.17 (m, 2H), 2.17 – 2.10 (m, 1H), 2.05 (s, 3H), 1.96 (t, J = 2.6 Hz, 1H), 1.55 – 1.40 (m, 8H), 1.29 (t, J = 7.1 Hz, 3H), 0.91 (t, J = 7.4 Hz, 3H).
^{13}C NMR (101 MHz, $CDCl_3$) δ 170.82, 166.29, 137.54, 129.62, 84.50, 80.67, 74.85, 68.48, 60.84, 59.09, 49.02, 33.56, 32.88, 28.51, 26.82, 24.48, 23.70, 18.36, 14.16, 9.36.

Supplementary data. All NMR spectra can be found in the Supporting information file.

Bibliography

(1) King, A. M.; Adams, M. J.; Carstens, E. B.; Lefkowitz, E. J. Virus Taxonomy. *Ninth Rep. Int. Comm. Taxon. Viruses* **2012**, *9*.

(2) Khanna, M.; Saxena, L.; Gupta, A.; Kumar, B.; Rajput, R. Influenza Pandemics of 1918 and 2009: A Comparative Account. *Future Virol.* **2013**, *8* (4), 335–342.

(3) Garten, R. J.; Davis, C. T.; Russell, C. A.; Shu, B.; Lindstrom, S.; Balish, A.; Sessions, W. M.; Xu, X.; Skepner, E.; Deyde, V.; others. Antigenic and Genetic Characteristics of Swine-Origin 2009 A (H1N1) Influenza Viruses Circulating in Humans. *science* **2009**, *325* (5937), 197–201.

(4) Palese, P. Influenza: Old and New Threats. *Nat. Med.* **2004**, *10* (12), S82–S87.

(5) Richard, M.; Fouchier, R. A. M. Influenza A Virus Transmission via Respiratory Aerosols or Droplets as It Relates to Pandemic Potential. *FEMS Microbiol. Rev.* **2015**, *40* (1), 68–85. https://doi.org/10.1093/femsre/fuv039.

(6) Asha, K.; Kumar, B. Emerging Influenza D Virus Threat: What We Know so Far! *J. Clin. Med.* **2019**, *8* (2), 192.

(7) Wei, X.; Pieters, R. J. Multivalency Effects in Neuraminidase Inhibitor Design for Influenza Virus. *Arkivoc* **2021**, *2021* (4), 1–16. https://doi.org/10.24820/ARK.5550190.P011.368.

(8) Wei, X.; Du, W.; Duca, M.; Yu, G.; de Vries, E.; de Haan, C. A. M.; Pieters, R. J. Preventing Influenza A Virus Infection by Mixed Inhibition of Neuraminidase and Hemagglutinin by Divalent Inhibitors. *J. Med. Chem.* **2022**, *65* (10), 7312–7323. https://doi.org/10.1021/acs.jmedchem.2c00319.

(9) Saito, N.; Komori, K.; Suzuki, M.; Morimoto, K.; Kishikawa, T.; Yasaka, T.; Ariyoshi, K. Negative Impact of Prior Influenza Vaccination on Current Influenza Vaccination among People Infected and Not Infected in Prior Season: A Test-Negative Case-Control Study in Japan. *Vaccine* **2017**, *35* (4), 687–693.

(10) Simonsen, L.; Taylor, R. J.; Viboud, C.; Miller, M. A.; Jackson, L. A. Mortality Benefits of Influenza Vaccination in Elderly People: An Ongoing Controversy. *Lancet Infect. Dis.* **2007**, *7* (10), 658–666.

(11) Daems, R.; Del Giudice, G.; Rappuoli, R. Anticipating Crisis: Towards a Pandemic Flu Vaccination Strategy through Alignment of Public Health and Industrial Policy. *Vaccine* **2005**, *23* (50), 5732–5742.

(12) Mckimm-Breschkin, J. L. Influenza Neuraminidase Inhibitors: Antiviral Action and Mechanisms of Resistance. *Influenza Other Respir. Viruses* **2013**, *7* (1 SUPPL.1), 25–36. https://doi.org/10.1111/irv.12047.

(13) Hay, A.; Wolstenholme, A.; Skehel, J.; Smith, M. H. The Molecular Basis of the Specific Anti-Influenza Action of Amantadine. *EMBO J.* **1985**, *4* (11), 3021–3024.

(14) Duwe, S. Influenza Viruses–Antiviral Therapy and Resistance. *GMS Infect. Dis.* **2017**, *5*.

(15) Abed, Y.; Boivin, G. A Review of Clinical Influenza A and B Infections with Reduced Susceptibility to Both Oseltamivir and Zanamivir. In *Open forum infectious diseases*; Oxford University Press, 2017; Vol. 4.

(16) Varghese, J. N.; McKimm-Breschkin, J. L.; Caldwell, J. B.; Kortt, A. A.; Colman, P. M. The Structure of the Complex between Influenza Virus Neuraminidase and Sialic Acid, the Viral Receptor. *Proteins Struct. Funct. Bioinforma.* **1992**, *14* (3), 327–332.

(17) Woods, J.; Bethell, R.; Coates, J.; Healy, N.; Hiscox, S.; Pearson, B.; Ryan, D.; Ticehurst, J.; Tilling, J.; Walcott, S. 4-Guanidino-2, 4-Dideoxy-2, 3-Dehydro-N-Acetylneuraminic Acid Is a Highly Effective Inhibitor Both of the Sialidase (Neuraminidase) and of Growth of a Wide Range of Influenza A and B Viruses in Vitro. *Antimicrob. Agents Chemother.* **1993**, *37* (7), 1473–1479.

(18) Kim, C. U.; Lew, W.; Williams, M. A.; Liu, H.; Zhang, L.; Swaminathan, S.; Bischofberger, N.; Chen, M. S.; Mendel, D. B.; Tai, C. Y.; Laver, W. G.; Stevens, R. C. Influenza Neuraminidase Inhibitors Possessing a Novel Hydrophobic Interaction in the Enzyme Active Site: Design, Synthesis, and Structural Analysis of Carbocyclic Sialic Acid Analogues with Potent Anti-Influenza Activity. *J. Am. Chem. Soc.* **1997**, *119* (4), 681–690. https://doi.org/10.1021/ja963036t.

(19) Limbani, B.; Bera, S.; Mondal, D. Synthetic Advancement of Neuraminidase Inhibitor “Tamiflu.” *ChemistrySelect* **2020**, *5* (20), 6083–6122. https://doi.org/10.1002/slct.202000675.

(20) Babu, Y. S.; Chand, P.; Bantia, S.; Kotian, P.; Dehghani, A.; El-Kattan, Y.; Lin, T.-H.; Hutchison, T. L.; Elliott, A. J.; Parker, C. D.; others. BCX-1812 (RWJ-270201): Discovery of a Novel, Highly Potent,

Orally Active, and Selective Influenza Neuraminidase Inhibitor through Structure-Based Drug Design. *J. Med. Chem.* **2000**, *43* (19), 3482–3486.
(21) Ikematsu, H.; Kawai, N. Laninamivir Octanoate: A New Long-Acting Neuraminidase Inhibitor for the Treatment of Influenza. *Expert Rev. Anti Infect. Ther.* **2011**, *9* (10), 851–857.
(22) Koyama, K.; Takahashi, M.; Nakai, N.; Takakusa, H.; Murai, T.; Hoshi, M.; Yamamura, N.; Kobayashi, N.; Okazaki, O. Pharmacokinetics and Disposition of CS-8958, a Long-Acting Prodrug of the Novel Neuraminidase Inhibitor Laninamivir in Rats. *Xenobiotica* **2010**, *40* (3), 207–216.
(23) Webster, R. G.; Bean, W. J.; Gorman, O. T.; Chambers, T. M.; Kawaoka, Y. Evolution and Ecology of Influenza A Viruses. *Microbiol. Rev.* **1992**, *56* (1), 152–179.
(24) Bernardi, A.; Jiménez-Barbero, J.; Casnati, A.; De Castro, C.; Darbre, T.; Fieschi, F.; Finne, J.; Funken, H.; Jaeger, K.-E.; Lahmann, M.; others. Multivalent Glycoconjugates as Anti-Pathogenic Agents. *Chem. Soc. Rev.* **2013**, *42* (11), 4709–4727.
(25) Pieters, R. J. Carbohydrate Mediated Bacterial Adhesion. *Bact. Adhes. Chem. Biol. Phys.* **2011**, 227–240.
(26) Branderhorst, H. M.; Ruijtenbeek, R.; Liskamp, R. M.; Pieters, R. J. Multivalent Carbohydrate Recognition on a Glycodendrimer-Functionalized Flow-through Chip. *ChemBioChem* **2008**, *9* (11), 1836–1844.
(27) Mammen, M.; Choi, S.-K.; Whitesides, G. M. Polyvalent Interactions in Biological Systems: Implications for Design and Use of Multivalent Ligands and Inhibitors. *Angew. Chem. Int. Ed.* **1998**, *37* (20), 2754–2794.
(28) Fasting, C.; Schalley, C. A.; Weber, M.; Seitz, O.; Hecht, S.; Koksch, B.; Dernedde, J.; Graf, C.; Knapp, E.-W.; Haag, R. Multivalency as a Chemical Organization and Action Principle. *Angew. Chem. Int. Ed.* **2012**, *51* (42), 10472–10498.
(29) Jencks, W. P. On the Attribution and Additivity of Binding Energies. *Proc. Natl. Acad. Sci.* **1981**, *78* (7), 4046–4050.
(30) Lu, W.; Pieters, R. J. Carbohydrate–Protein Interactions and Multivalency: Implications for the Inhibition of Influenza A Virus Infections. *Expert Opin. Drug Discov.* **2019**, *14* (4), 387–395. https://doi.org/10.1080/17460441.2019.1573813.
(31) Pertici, F.; de Mol, N. J.; Kemmink, J.; Pieters, R. J. Optimizing Divalent Inhibitors of Pseudomonas Aeruginosa Lectin LecA by Using a Rigid Spacer. *Chem. Eur. J.* **2013**, *19* (50), 16923–16927.
(32) Gestwicki, J. E.; Cairo, C. W.; Strong, L. E.; Oetjen, K. A.; Kiessling, L. L. Influencing Receptor- Ligand Binding Mechanisms with Multivalent Ligand Architecture. *J. Am. Chem. Soc.* **2002**, *124* (50), 14922–14933.
(33) Kiessling, L. L.; Gestwicki, J. E.; Strong, L. E. Synthetic Multivalent Ligands as Probes of Signal Transduction. *Angew. Chem. Int. Ed.* **2006**, *45* (15), 2348–2368.
(34) Varghese, J. N.; Chandana Epa, V.; Colman, P. M. Three-Dimensional Structure of the Complex of 4-Guanidino-Neu5Ac2en and Influenza Virus Neuraminidase. *Protein Sci.* **1995**, *4* (6), 1081–1087.
(35) Macdonald, S. J.; Watson, K. G.; Cameron, R.; Chalmers, D. K.; Demaine, D. A.; Fenton, R. J.; Gower, D.; Hamblin, J. N.; Hamilton, S.; Hart, G. J.; others. Potent and Long-Acting Dimeric Inhibitors of Influenza Virus Neuraminidase Are Effective at a Once-Weekly Dosing Regimen. *Antimicrob. Agents Chemother.* **2004**, *48* (12), 4542–4549.
(36) Fu, L.; Bi, Y.; Wu, Y.; Zhang, S.; Qi, J.; Li, Y.; Lu, X.; Zhang, Z.; Lv, X.; Yan, J.; Gao, G. F.; Li, X. Structure-Based Tetravalent Zanamivir with Potent Inhibitory Activity against Drug-Resistant Influenza Viruses. *J. Med. Chem.* **2016**, *59* (13), 6303–6312. https://doi.org/10.1021/acs.jmedchem.6b00537.
(37) Yan, Z. L.; Liu, A. Y.; Wei, X. X.; Zhang, Z.; Qin, L.; Yu, Q.; Yu, P.; Lu, K.; Yang, Y. Divalent Oseltamivir Analogues as Potent Influenza Neuraminidase Inhibitors. *Carbohydr. Res.* **2019**, *477*, 32–38. https://doi.org/10.1016/J.CARRES.2019.03.012.
(38) Gubareva, L. V.; Sleeman, K.; Guo, Z.; Yang, H.; Hodges, E.; Davis, C. T.; Baranovich, T.; Stevens, J. Drug Susceptibility Evaluation of an Influenza a(H7n9) Virus by Analyzing Recombinant Neuraminidase Proteins. *J. Infect. Dis.* **2017**, *216*, S566–S574. https://doi.org/10.1093/infdis/jiw625.
(39) Yu, G.; Vicini, A. C.; Pieters, R. J. Assembly of Divalent Ligands and Their Effect on Divalent Binding to Pseudomonas Aeruginosa Lectin LecA. *J. Org. Chem.* **2019**, *84* (5), 2470–2488.

(40) Nie, L. D.; Shi, X. X.; Kwang, H. K.; Lu, W. D. A Short and Practical Synthesis of Oseltamivir Phosphate (Tamiflu) from (-)-Shikimic Acid. *J. Org. Chem.* **2009**, *74* (10), 3970–3973. https://doi.org/10.1021/jo900218k.
(41) Karpf, M.; Trussardi, R. Efficient Access to Oseltamivir Phosphate (Tamiflu) via the O-Trimesylate of Shikimic Acid Ethyl Ester. *Angew. Chem. - Int. Ed.* **2009**, *48* (31), 5760–5762. https://doi.org/10.1002/anie.200901561.
(42) Mooney, C. A.; Johnson, S. A.; 'T Hart, P.; Quarles Van Ufford, L.; De Haan, C. A. M.; Moret, E. E.; Martin, N. I. Oseltamivir Analogues Bearing N-Substituted Guanidines as Potent Neuraminidase Inhibitors. *J. Med. Chem.* **2014**, *57* (7), 3154–3160. https://doi.org/10.1021/jm401977j.
(43) Kalashnikov, A. I.; Sysolyatin, S. V.; Sakovich, G. V.; Sonina, E. G.; Shchurova, I. A. *Facile Method for the Synthesis of Oseltamivir Phosphate*; 2013.
(44) Kuang, J.; Xie, X.; Ma, S. A General Approach to Terminal Allenols. *Synthesis* **2013**, *45* (05), 592–595. https://doi.org/10.1055/s-0032-1317949.
(45) Abrams, S. R.; Shaw, A. C. *On the Mechanism of 1,3-Prototropic Shifts in Acetylene-Allene Isomerizations1*; UTC, 1987; Vol. 52, p 12. https://pubs.acs.org/sharingguidelines.
(46) Abrams, S. R. Alkyne Isomerization Reagents: Mixed Alkali Metal Amides. *Can. J. Chem.* **1984**, *62* (7), 1333–1334.
(47) Rohloff, J. C.; Kent, K. M.; Postich, M. J.; Becker, M. W.; Chapman, H. H.; Kelly, D. E.; Lew, W.; Louie, M. S.; McGee, L. R.; Prisbe, E. J.; others. Practical Total Synthesis of the Anti-Influenza Drug GS-4104. *J. Org. Chem.* **1998**, *63* (13), 4545–4550.
(48) Xu, D.; Li, Z.; Ma, S. Novozym-435-Catalyzed Enzymatic Separation of Racemic Propargylic Alcohols. A Facile Route to Optically Active Terminal Aryl Propargylic Alcohols. *Tetrahedron Lett.* **2003**, *44* (33), 6343–6346. https://doi.org/10.1016/S0040-4039(03)01528-4.
(49) Ortiz, C.; Ferreira, M. L.; Barbosa, O.; dos Santos, J. C.; Rodrigues, R. C.; Berenguer-Murcia, Á.; Briand, L. E.; Fernandez-Lafuente, R. Novozym 435: The "Perfect" Lipase Immobilized Biocatalyst? *Catal. Sci. Technol.* **2019**, *9* (10), 2380–2420.